2013

Using Data Assimilation To Investigate The Effect Of African Easterly Waves, Mesoscale Convective Systems, And Orography On Tropical Cyclogenesis Over Eastern Pacific

Gregory N. Terkper
North Carolina Agricultural and Technical State University

Using Data Assimilation to Investigate the Effect of African Easterly Waves, Mesoscale Convective Systems, and Orography on Tropical Cyclogenesis over Eastern Pacific

Gregory N. Terkper

North Carolina A&T State University

A thesis submitted to the graduate faculty

in partial fulfillment of the requirements for the degree of

MASTER OF SCIENCE

Department: Mathematics

Major: Applied Mathematics

Major Professor: Dr. Guoqing Tang

Greensboro, North Carolina

2013

School of Graduate Studies
North Carolina Agricultural and Technical State University
This is to certify that the Master's Thesis of

Gregory N. Terkper

has met the thesis requirements of
North Carolina Agricultural and Technical State University

Greensboro, North Carolina
2013

Approved by:

Dr. Guoqing Tang Major Professor	Dr. Yuh-Lang Lin Committee Member
Dr. John Paul Roop Committee Member	Dr. Yevgeniy A. Rastigeyev Committee Member
Dr. Guoqing Tang Department Chair	Dr. Sanjiv Sarin Dean, The Graduate School

Biographical Sketch

Gregory N. Terkper was born in Preastea western region of Ghana on June 17, 1979. He received his Bachelor of Education degree in Mathematics from the University of Cape Coast Ghana in 1996. He began his graduate research in summer 2010 with Dr. Guoqing Tang, Dr. John Paul Roop and Dr. Yuh-Lang Lin. Gregory will earn a Master of Science in Applied Mathematics from North Carolina A&T State University in spring 2013.

Dedication

I dedicate this Thesis to my wife and my new born son, Peter Kofi Terkper II, for their encouragement and support.

Acknowledgements

This thesis would not have been possible without the support of many people. I would like to thank my advisor, Dr. Guoqing Tang, for his encouragement, guidance and support throughout this research and my program. I would also express my gratitude to Dr. Yuh-Lang Lin and Dr. J. P. Roop for their advice and training on WRFVAR. My gratitude also goes to other members of my thesis advisory committee and the mathematics department graduate faculty. I would also like to say special thanks to my fellow graduate students, James Spinks, Van Thu Thi Nguyen and Matthew Hairston, for assisting me with WRF, GrADS scripts and Linux.

Table of Contents

List of Figures

List of Tables

List of Abbreviations

3DVAR	Three-Dimensional Variational Data Assimilation
4DVAR	Four-Dimensional Variational Data Assimilation
AEJ	African easterly jet
AEW	African Easterly Waves
AOAWS	Advanced Operational Aviation Weather System
ECMWF	European Center for Medium-range Weather Forecasts
GFS	Global Forecasting System
GrADS	Grids Analysis and Display System
IR	Infrared
ITCZ	Intertropical Convergence Zone
LIN	Lin et al
MCS	Mesoscale Convective System
MJO	Madden-Julian Oscillation
MM5	The fifth generation NCAR/Penn State Mesoscale Model
MRG	Mixed Rossby-Gravity Waves
MSLP	Minimum Sea Level Pressure
MP	Microphysics
NCAR	National Center for Atmospheric Research
NCEP	National Center for Environmental Prediction
NHC	National Hurricane Center
NOAA	National Oceanic and Atmospheric Administration
NWP	Numerical Weather Prediction

OI	Optimal Interpolation
OLR	Outgoing longwave radiation
RRTM	Rapid Radiative Transfer Model
SSHS	Saffir–Simpson hurricane scale
TC	Tropical Cyclone
TS	Tropical Storm
VAR	Variational
WRF	Weather Research and Forecasting Model
WRF-ARW	Advanced Research - WRF
WRFDA	Weather Research and Forecasting Model Data Assimilation
WSM6	WRF Single-Moment 6-class Microphysics

Abstract

This study examines the association of tropical cyclogenesis and tropical wave activities such as African Easterly Waves (AEWs) in the Northeast Pacific Ocean. The impact of Central and Mexico Mountains on hurricane genesis, intensification and track is also studied in this paper. Eight numerical simulations using Weather Research and Forecasting (WRF-ARW) model are conducted to investigate the genesis, track and intensification of Hurricane Jimena (2009) a category 4 (on the Saffir-Simpson Hurricane Scale) hurricane during the 2009 eastern Pacific hurricane season. In addition, this study also analyzes the impact of three dimensional variational data assimilation of (3DVAR) of NCEP FNL data on WRF simulations.

Based on satellite imagery and WRF analysis of Hurricane Jimena (2009), we find that the formation of Jimena on August 28, 2009 was trigged by a tropical wave from off the coast of Africa and propagated west-ward, across the Atlantic, Caribbean and into eastern Pacific on August 25. The study also reveals that initial time (or initial conditions) and microphysics scheme along with data assimilation play an important role on WRF-ARW model simulation.

CHAPTER 1

Introduction

Observations indicate that averagely about 16 tropical storms (maximum sustained winds of 39 to 73 mph (34 to 63 knots) are formed in the North Eastern Pacific basin each year. About 56 percent of these named systems strengthen into hurricanes (maximum sustained winds of 74 mph (64 knots) or higher) and 4 approximately grow into major hurricanes (maximum sustained winds of 111 mph (96 knots) or higher) in this basin. Numerous studies have attributed the development of tropical cyclones in this basin to easterly waves. The easterly waves are also known as African easterly waves which are produced over east of Africa, and propagate westward across the Atlantic through the Caribbean and into the eastern pacific (Avila & Pasch, 1992; Molinari & Vollaro, 2000). Majority of these tropical cyclones are developed close to the lee side of Mexico and Central America probably due to the interaction of the waves with large-scale of mountain ranges in this region.

Pacific hurricane refers to a hurricane or a storm formed in the Eastern North Pacific (term as tycoon in the Western North Pacific). This basin which is located on the lee side of Mexico and Central America mountains is one of the world most active regions for tropical cyclone activity (Bowman & Renard, 1976). The Pacific hurricane season runs from May 15th to November, 30 with August being its peak. Most tropical cyclones in Eastern Pacific tend to intensify quickly compared to the Atlantic Hurricanes. Moreover, TCs in the Eastern North pacific usually dominate in the number of cyclogenesis. Figure 1 is a comparison of number of cyclones from the beginning of the hurricane season to the end of August for the Eastern Pacific hurricane with that of Atlantic hurricane. With the exception of the year 1779, 1995, 1997 and 1997 the north east pacific basin seems to be more active compared with that of Atlantic basin.

The Figure also shows the number of cyclones for the north east pacific is about three times greater than the Atlantic cyclones for 2009 from May 15 to the August 31. The North Eastern Pacific basin was extremely active in August 2009 according to the NHC report for 2009 hurricane season. Seven tropical storms were formed in August and three of them became hurricanes and then grew into a major hurricane. Their report also indicates that since 1985, this is the first time 7 tropical storms have developed in any month in this region. Moreover, since 1998 no basin has recorded the formation of three major hurricanes in any month.

Most of the tropical cyclones in Eastern pacific tend to intensify quickly compared to the Atlantic Hurricanes. Like the Atlantic hurricanes, Pacific hurricanes usually tend to propagate west and then may turn northward. The locations of tropical cyclogenesis are said to be scattered throughout tropical Atlantic whiles those of the eastern pacific are localized close to west of the Sierra Madre Mountains in Central America (Bowman and Renard 1976). Zehnder et al. in1991 observed that out of the 157 tropical cyclones that were developed in eastern North Pacific, 109 of them were generated in the region bounded by 10^{o}N and 20^{o}N, 110^{o}W and west of the coast of Mexico. He suggested that the high incidences of tropical cyclones activities in this basin may be a result of initial disturbances generated from baroclinic flow with the mountain range in that territory. Similarly, Farfan and Zehnder 1997 demonstrated the initial circulation that spawned Hurricane Guillermo (1991) was a result of interaction of an easterly wave in the Caribbean Sea with the Central America mountains range.

Warm sea surface temperature at least 26.5 degree celsius, weak vertical wind shear at most 10 m/s, significant large planetary vorticity, a near-surface preexisting disturbance with sufficient vorticity(e.g. tropical waves) and relatively moist middle troposphere are a few of the necessary conditions for TC development Lin (2007). Contrarily, development of TCs in this

region is limited by increased vertical wind shear west of 120W and cyclones that move northward dissipate due to lower sea surface temperatures (Gary 1968) and dry air. Tropical cyclones in this region usually are interrupted by eye wall replacement cycle. Unlike Hurricane Jimena (2009) which strengthened to a peak intensity of 135 kt in less than 18 hours, most of the storms that undergo eyewall replacement cycle weaken and dissipate afterward.

Easterly waves which later amplify into tropical storms (Dunn, 1940; Miller, 1991) appear to be the source of initial circulations of majority of east Pacific tropical storms (Raymond and López - Carrillo, 2006). Avila and Pasch (1992) stated that these tropical waves move westward from Africa into the eastern pacific through Atlantic and the Caribbean. They traced each of the 1991 eastern pacific cyclones back to African easterly waves that set off the coast of West Africa. Satellite data and tropical cyclone reports by National Hurricane Center also indicate that most of the eastern tropical cyclones were originated from Africa or Cape Verde Island. Shapiro (1986) gave specific examples of how such propagation occurs. In addition, some of the cyclones in this region are remnants of the Atlantic tropical cyclones. Avila stated in the August 2009 Tropical Cyclone Report of Tropical Storm Ignacio that Ignacio was formed from the same tropical wave that spawned Tropical Storm Ana in the Atlantic basin. These disturbances were weak and disorganized at the initial stage with little or no convection; however they gradually developed into a tropical depression or storm or hurricane once they reach environment favorable for TC formation.

Mesoscale convective systems (MCSs) that are embedded within the Africa Easterly have also been associated to tropical cyclogenesis by numerous researchers. Lin (2007, p. 322) described MCSs as organized clusters of thunderstorms, which persist at least for several hours that produce a contiguous precipitation region. Some of the tropical cyclones that occur in the

eastern North Pacific were initiated by MCSs formed over the mountains and propagated westward (Velasco and Fritsch 1987; Zehnder and Gall 1991; Zehnder and FARFA´N, 1991). Lin et al (2001) explained how tropical cyclogenesis are triggered by tropical disturbance as follows: First of all, TC disturbances are formed as an MCS and as the TC precursors which consist of easterly waves embedded with MCs propagate over the ocean they may interact with other eastward systems, such as Madden-Julian Oscillation (MJO), monsoon trough, and Kelvin waves. Subsequently, vertical hot towers or convective vortices are produced from cumuli embedded within the MCSs if the region posses favorable conditions. Also these hot towers may interact and merge with other vortices to form a larger cyclonic vortex. Finally the vortex may develop into a tropical depression if necessary conditions are met.

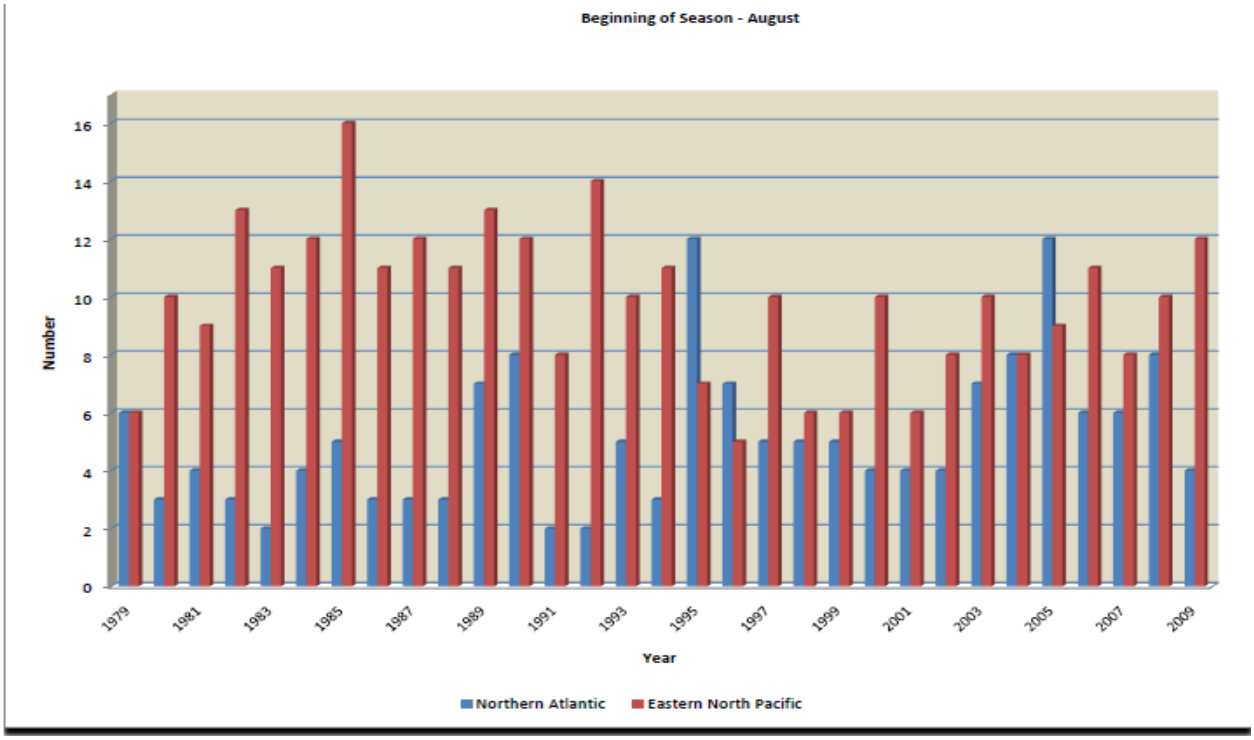

*Figure 1.*Tropical Cyclones from the beginning of the Season to August (1979 to 2009). Blue and red bar represent the total number of Northern Atlantic and Eastern North Pacific Tropical Cyclones respectively.

Several researchers have proposed and used the following major mechanisms to explain tropical cyclone development: cooperative intensification mechanism, linear Conditional Instability of the Second Kind (CISK) mechanism, wind-induced surface heat exchange (WISHE) mechanism, vortex interaction mechanism, hot tower mechanism and preexisting disturbances mechanism (Cf. Lin et al., 2001 for detail explanation of the above mechanisms). Other researchers have also proposed a variety of mechanism for wave intensification and cyclogenesis. Baroclinic conversions (Thorncroft and Hoskins 1994b), interaction of the wave with another atmospheric disturbance (Shapiro, 1977; Raymond, and López-Carrillo, 2006), interaction of wind surge with disturbance (Lee, 1989), interaction of waves with mountain etc are some of the proposed mechanisms.

This research studies the orographic effects on the cyclogenesis of Hurricane Jimena (2009) using the version 3.3 of the Weather Research and Forecasting (WRF) model in conjunction with its data assimilation system (WRFDA). This study examines the association of tropical cyclogenesis and tropical wave activities such as African Easterly Waves (AEWs) in the Northeast Pacific Ocean. The impact of Central and Mexico Mountains on hurricane genesis, intensification and track is also studied in this paper. Eight numerical simulations using Weather Research and Forecasting (WRF-ARW) model are conducted to investigate the genesis, track and intensification of Hurricane Jimena (2009). In addition, this study also analyzes the impact of three dimensional variational data assimilation of (3DVAR) of NCEP FNL data on WRF simulations.

Data assimilation is the process whereby observational data is incorporated into the WRF modeling in order to obtain suitable set of data to initialize a model (Holton 2004). The aim of a data assimilation scheme is to use measured observations in combination with a dynamical

system model in order to derive accurate estimates of the current and future states of the system, together with estimates of the uncertainty in the estimated states. Bouttier and Courtier (1991) categorized it into two basic approaches, namely, sequential assimilation and retrospective assimilation. The former approach, like the real-time assimilation systems, considers observation made in the past until the time of analysis while the latter uses observation from the future.

Based on satellite imagery and WRF analysis of Hurricane Jimena 2009, we find that the formation of Jimena on August 28, 2009 was trigged by a tropical wave from off the coast of Africa and propagated west-ward, across the Atlantic, Caribbean and into eastern Pacific on August 25. The study also reveals that initial time (or initial conditions) and microphysics scheme play an important role on WRF-ARW model simulation.

Out of the seventeen named storms that developed during the 2009 eastern Pacific hurricane season, seven became hurricanes, of which four attained major hurricanes status, and two of the tropical depressions formed could not grow into a tropical storm. Two TCs, Hurricane Jimena (2009) and Hurricane Rick (2009), made a landfall. Three of the storms recorded four deaths associated with large waves and flash water flooding caused by these storms. Hurricane Jimena (2009) is the second largest tropical cyclone to make landfall in this region since 1971 (Hurricane Linda of 1997 was stronger) and the first storm to make landfall during the 2009 Pacific hurricane season. Hurricane Jimena (2009)'s origin can be traced back to a tropical wave that moved west-ward off the coast off West Africa, crossed the Central America and entered eastern North Pacific on August 25. NHC stated that shower activities increased on August 27 and high probability of devolvement was issued less than 24 hours before it originated on 1800 UTC 28 August. The storm rapidly intensified and reached its peak intensity of 135 knot by 1800 UTC 31 August. Hurricane Jimena (2009) made its first landfall as a category 2 hurricane

on the Saffir–Simpson hurricane scale (SSHS) on 1200 UTC 2 September over Isla Santa Margarita, Baja California del Sur. It dissipated on September 5 after it made three more landfalls at Puerto San Carlos, Baja California del Sur, east of San Juanico in Baja California del Sur and near Santa Rosalia, Baja California del Sur. Ten thousands of dollars were reported in damages as a result of strong wind and fresh water floods.

The paper is organized as follows. Chapter 2 provides an overview of results from previous researches related to orographic influence on the cyclogenesis, of Pacific hurricanes and their associations with AEWSs/MCSs. The experimental design are described in Chapter 3 and an overview of 3D Variational is presented in Chapter 4.The topography of the Eastern Pacific ocean, synopsis environments of Hurricane Jimena 2009, WRF-ARW model are also discussed. Results from the numerical simulation are compared with observed data, satellite imagery in Chapter 5. Finally, the summary of this research and future work is presented in chapter 6.

CHAPTER 2

Literature Review

African easterly waves are westward traveling disturbances that have their origins over North Africa (Riehl 1945) and usually they propagate across tropical northern Africa between May and October (GRIST, 2001). These disturbances occur primarily during the summer season sometimes developing into tropical cyclones over the Western Atlantic (Estoque et al., 1982). Carlson (1969a, b) discovered that many wavelike disturbances developed in a vicinity east of the Greenwich meridian and propagated westward to south of the surface convergence zone in the southern Sahara. The study of the origin and structure of easterly waves in the lower troposphere of North Africa by Burpee (1972) shows that the AEWs relates directly to mid-tropospheric easterly jet that is found within baroclinic zone. In otherwise, these waves originate over Africa and are as the result of baroclinic instability of African easterly jet.

Avila and Pasch (1992), and Landsea et al. (1998) suggested that AEWs provide the requisite forcing for tropical cyclogenesis and they modulate West African rainfall, including mesoscale convective systems (MCSs) (Fink and Reiner 2003). Spinks (2009), listed the following as basic characteristics of AEWs; a propagation speed of 7 – 9 ms-1, a wavelength of ~2000 – 4000 km, and propagating along the rainy zone and to the south of the African easterly jet (AEJ) around 10^{o}N (AEWs) or along the Saharan thermal low near 20^{o}N (AEWn) and also associated this to pre-Alberto (2000) AEWS (Lin et al., 2005), the pre-Helene (2006) AEWS propagated along 10^{o}N. Usually, the waves have a period of about 3 or 4 days and a wavelength of 2000 to 2500 km (Burpee 1974). These characteristics may differ from region to region or longitude (Reed et al. 1977). Estoque et al. (1983) wrote “Observational data indicate that the waves are most intense near the 700 mb level where the perturbations in the meridional wind

component attain magnitudes of about 5 ms-^{1}". Carlson (1969 b) analyzed 2,000 to 10,000-ft streamlines daily over West Africa for a three and half month period starting in July 1968 and concluded that the disturbances are large-scale (synoptic) wave perturbations with considerable latitudinal extent that exist apart from the ITC region, although they extend into that area.

In 2005, Frank and Roundy used daily wind estimates for 850hPa, 200hPa and outgoing longwave radiation (OLR) data from 1974-2002 to analyzes relationships between the major tropical wave types and tropical cyclogenesis in all six major tropical cyclone basins (North Indian, South Indian, Northwest Australia and South Pacific, Northwest pacific, Northeast pacific and North Atlantic). Their research provided evidence that tropical wave perturbations are associated with tropical cyclogenesis. Their study revealed that easterly waves, MJO, equatorial Rossby waves and mixed Rossby-gravity (MRG) waves play a significant role in the development of many tropical cyclones that are formed annually. Also their result indicates AEWs enhances genesis by increasing large-scale convection and low-level rotation in the region. Moreover they found out that most of the tropical cyclones form within or very close to the circulations of monsoon trough ITCZs. Finally they stated that MRG and Africa easterly waves active in the northeast Pacific during the cyclone season compare the other month.

These AEWs usually are accompanied by mesoscale convective systems (MCSs), which cross the center Sahel region between 8^{o} N – 18^{o}N and 10^{o}W - 17^{o}E and dissipate in the tropical Atlantic Ocean towards 20^{o}W (Kouadio et al. 2010). Researchers such as Simpson et al., 1968; Carlson, 1969a, with the aid of satellite data proved that mesoscale convective complexes (MCCs) its associated AEWs can spawn tropical cyclogenesis (Robertson, 2004). The connective vortices or hot towers associated with the MCSs might have served as precursor for the tropical depression over the eastern Atlantic Ocean that eventually became Hurricane Alberto

(2000).

Zehnder et al. (1999) examine the relation between easterly waves that propagate from over the Caribbean Sea towards the East Pacific Ocean and deep convective bursts that frequently occur over the Gulf of Tehuantepec which often intensify into tropical cyclones. This study shows that the disturbances present over the Caribbean have a horizontal and vertical structure and propagation features similar to easterly waves. About 60 AEWSs emerging from the west coast of Africa each summer (Avila and Clark 1988) based on observation from the Tropical Prediction Center.

The North East Pacific basin is one of the regions with world's most intense cyclonic activities. These cyclonic activities originate from African easterly waves as mentioned early on and propagate from North Africa towards the tropical Atlantic and Central America. Molinari et al. (1999) stated "the eastern Pacific ocean is the most active tropical cyclone formation region on earth in terms of genesis events per unit area and per unit time". Easterly waves account for about 60% the Atlantic tropical storms and almost all the tropical cyclones that occur in the Eastern Pacific Ocean. During the 1992 hurricane season, 73 tropical waves the northwest coast of Africa and moved west-ward over the tropical Atlantic, the Caribbean, and Central America and into the eastern Pacific (Avila and Pasch 1992). The average period of these waves is about 2.9 days. A large number of the waves did become convectively active in the eastern Pacific, where weaker than normal vertical shear prevailed south of 15N, likely leading to formation of the majority of the 1991 tropical cyclones in that basin. Several other researchers also have conducted studies on the association of AEW-MCSs and topical cyclogenesis over the North Eastern Pacific.

Frank and Clark (1980) also suggested the formation of eastern Pacific tropical cyclones

from African wave. Tai and Ogura (1986) in their study investigated wave disturbances over the eastern Pacific using MEM spectral analysis and showed that lower level waves with a period of 4-6 days are active in both the eastern and western Pacific. Also they observed that growth rate of waves in this region is smaller than those of other region which indicates less strong wave activities compared to the other regions. In addition, Molinari et al. (1999) investigated the genesis of Hurricane Hernan (1996) in the eastern Pacific using gridded analyses from the European Centre for Medium-Range Weather Forecasts and gridded outgoing longwave radiation. Their study revealed that Hurricane Hernan (1996) was trigged by easterly waves that could be track back to Africa. They also demonstrated that interaction of the Central American mountains with African Easterly waves played a vital role in cyclogenesis and proposed that the likelihood of eastern Pacific cyclogenesis is determined by the strength of the waves reaching the Central America. Thus, if strong waves cross the mountains and if favorable sea surface temperatures present, and small vertical wind shear, cyclogenesis is likely.

Merkine (1975) demonstrated that baroclinic instabilities on the lee of a mountain range were caused by intensification of shears downstream. This was initiated by interaction of a flow vertical shear upstream and topography. Zehnder et al. (1999) again, using numerical integration of the shallow water equations on an equatorial beta-plane channel investigated the interaction of an idealized easterly wave with an orographic feature representing the Sierra Madre of Mexico and a large-scale, meridional sheared zonal flow representing the ITCZ in the eastern North Pacific. Zehnder et al associated the tropical cyclogenesis in the eastern Pacific to the interaction of an easterly wave, the mountains of Central America and Mexico, and the ITCZ. The study shows the relative vorticity formed in the lee of the terrain was as a result of the interaction of an easterly wave with the terrain attributed to the net deflection of parcels by the mountain

anticyclone described by Zehnder (1991). In 2004 also suggested that mountain waves created by flow over large mountain can produce orographic disturbances in 10 to 100-km mesoscale range.

Data assimilation systems are used to provide a better estimate of the atmospheric state (the analysis) at a given time from a range of observation systems, supplemented with information from previous forecasts or analyses, error statistics, and laws of physics (Fan et al 2004). Data assimilation was described by Lorenc et al (2007) as the best and affordable NWP method to determine the initial state of the atmosphere from observation. Cucurull et al (2004) analyzed the impact of the 3DVAR of GPS ZTD observations during the evolution of a mesoscale convective system that affected the western Mediterranean during 14–15 December 2001. The experiments show that the 3DVAR system in a cycling mode improved the model analysis and weather prediction with the use of local meteorological and GPS observations significantly. Barker et al (2004) observed a significant improvement in forecast wind score, especially for the higher-resolution domains using 3DVAR in the Advanced Operational Aviation Weather System (AOAWS).

However, they reported minimal improvement in temperature and humidity scores. Fan et al (2004) investigated the impacts of horizontal resolution on the 3DVAR and MM5 forecasts. Like the findings of Barker et al, their result show that experiment with higher resolution and application of 3DVAR in a cycling mode with MM5 significantly improves the model simulations. Several researchers (e.g., Lewis and Derber 1985; Courtier and Talagrand 1987:

Thepaut et al.1993; Zupanski 1993; Kuo et al. 1996; Zupanski 1997 and GUO et al. 2000) have reported encouraging result using the variational approach.

CHAPTER 3

Methodology

3.1 Topography

The Pacific Ocean which measures about 63.8 million square miles is the world's largest ocean and it is subdivided into North and South Pacific Ocean by the equator. North Eastern region encompasses the area from west coast of North America to 140W. Series of large-scale mountain ranges stretch along Pacific Ocean coast of North America from northern British Columbia (Canada) to northwestern Mexico. The genesis of majority of Pacific hurricanes can be located in an area close to the Sierra Madres. Sierra Madres consists of the Sierra Madre Occidental (to the west) the longest with some of it peaks rising above 1.5km, the Sierra Madre Oriental (to the east), and the Sierra Madre del Sur (to the south see Figure 2).This ridge has a width of about 600km and it extend from US-Mexico border in the northwest to approximately 15^{o}N in the southeast (Zehnder et al., 1991). The eastern Pacific is one of the most extensive, deep cloud active regions around the tropical oceans, especially, during summer season.

Figure 2. Topography of North East Pacific provided by graphic.com.

3.2 Hurricane Jimena (2009) Synopsis

John L. Beven of the National Hurricane Center, reported that hurricane Jimena(2009) was a high-end category 4 hurricane (on the Saffir-Simpson Hurricane Scale) with maximum sustained wind about 155mph and minimum surface pressure near 931mbar. It was the second strongest tropical cyclone of the 2009 Pacific Hurricane season. Hurricane Jimena (2009) developed during the late hours of August 28, off the Western coast of Mexico. Jimena was formed from a tropical wave that moved off the west coast of Africa on August 15, 2009. The system traveled westward across the Atlantic, through the Caribbean, over the Central America mountains and entered into the eastern Pacific basin on August 25.

The Atmospheric Infrared Sounder (AIRS) instrument on NASA's Aqua satellite captured the two areas on August 27at 5:23 p.m. EDT. Figure 3 shows the organization of Jimena from August 27- 30 obtain from AIRS. The purple color clouds depict cloud top temperature of minus 63F (220K) or below and highest thunderstorm cloud tops whiles blue

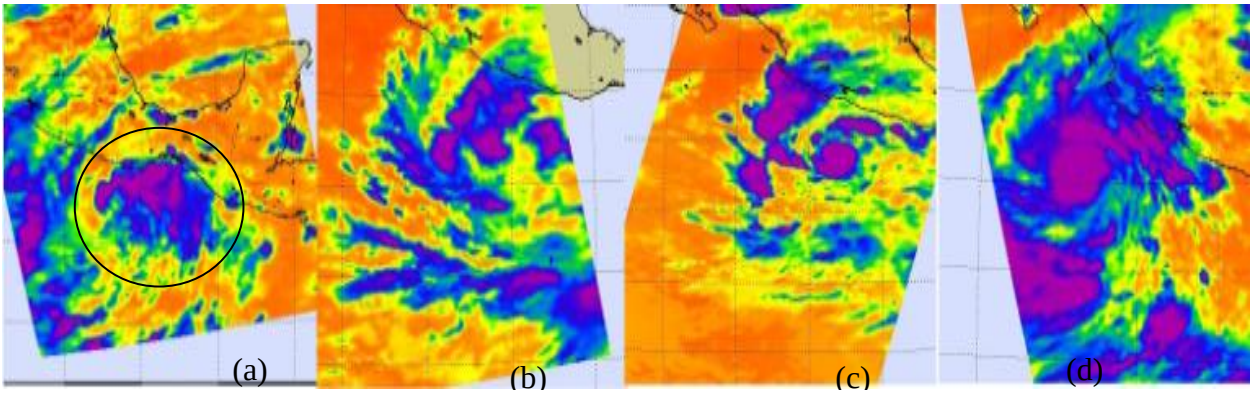

Figure 3. Compilation of Atmospheric Infrared Sounder (AIRS) explosive growth of Hurricane Jimena in the Eastern Pacific Ocean from August 27 to 30, 2009. (a) August 27, (b) August 28, (c) August 29 and (d) August 30. Purple area mark highest thunderstorm cloud top with cloud temperature as cold as 220 Kelvin (-63f) or less and the blue area mark clouds temperature 240 Kelvin (-27F) and above. Credit: NASA/JPL, Ed Olsen.

mark minus 27F (240K). The satellite imagery in Figure 3(d) shows that Jimena's cloud top temperatures were colder than minus 63F indicating powerful thunderstorms in her center (Rob Gutro). Shower and thunderstorm activity began to increase on August 27. Although both areas were disorganized, the National Hurricane Center reported on Friday, August 28 that the chance for development is at least 50%. The first area of disorganized showers and thunderstorms is associated with low pressure, which later developed into Hurricane Jimena, was located a couple of hundred miles south of Acapulco, Mexico (see Figure 3a area in the circle). The second area of showers and thunderstorms are further west, about 950 miles south-southwest of the southern tip of Baja California later developed and became Tropical Storm Kelvin.

The system (the first area) became Tropical Depression 13- E on August 28 1800 UTC about 190 mi south of Acapulco (Figure 3b). It strengthened into a Tropical Storm early on 29 August with maximum sustained winds near 70 mph and later attained hurricane status on the same day. She was more rounded and well organized with increasing thunderstorms (Figure 3.c). Her intensification was fueled by light upper level winds and warm sea surface temperatures (Rob Gutro, NASA/Goddard Space Flight Center). Initially the depression propagated westward on the south side of a mid-level ridge over Mexico but later turned northwestward on August 30. Hurricane Jimena strengthened to a category four hurricane on the Saffir-Simpson Scale with estimated intensity of 120 knot on August 30.

The rapid intensification of Hurricane Jimena continued until the development was interrupted by an eyewall replacement cycle. After the cycle completed early on 31st August, Jimena again quickly intensified to the peak of 135 knot (145 mph) by 1800 UTC on the same day. Small radius of maximum winds embedded within the depression at the time of genesis possible contributed to the rapid intensification. Two NASA satellites confirmed that Jimena had

organized cloud cover and very heavy rain and thunderstorms were reported on August 31. The center of Jimena was about 355 miles south-southeast of Cabo San Lucas, Mexico, near 18.0^{o} N and 108.3^{o} W. Figure 4 is the NHC "best track" chart which shows Jimena's path from August 28 to September 5, 2009.

Strong vertical wind shear, low sea surface temperatures and a second eyewall replacement contributed to the weakening of Jimena early on September 1st. Jimena made landfall over Isla Santa Margarita, Baja California del Sur, about 1200 UTC on the 2nd of September as a category 2 hurricane with estimated intensity of 90 knot and a pressure of 971 mbar which ties it with Hurricane Norbert of 2008 as the strongest land falling hurricane recorded on the west coast of Baja California. A second landfall at the same magnitude occurred an hour later at Puerto San Carlos, Baja California del Sur. The storm was downgraded to category 1 before it made a third landfall just east of San Juanico in Baja California del Sur at about 2100 UTC 2 September.

By the late September 3, Hurricane Jimena (2009) had reduced to a tropical storm and started a southwestward motion later that day. The storm became a tropical depression the next day before she made her final landfall near Santa Rosalia, Baja California del Sur with wind of 30 mph. The depression degenerated to a remnant low while it crossed Baja, with the low dissipating over the Pacific on 5 September. It dissipated on 5 September after it made its' fourth landfall near Santa Rosalia, Baja California del Sur with wind of 30 mph. Table 1 highlight the various stages, the time, location, wind speed in knot and pressure (mb) of Jemina from August 28 to September 5. Severe wind and rain contributed to wild spread of flash water floods in Mulege, Baja California del Sur. Interaction with land, increasing, vertical shear, cooler waters, and second eye wall replacement cycle contributed to the weakening of the Jimena (T.B.

Kimberlain and M.J. Brennan, 2011). NHC stated that one death was reported and ten thousands of dollars lost in damage to building and property.

The maximum reported storm-total rainfall was 26.46 inches at Guaymas in Sonora. Table 12 in appendix D lists the rainfall total of affected areas.

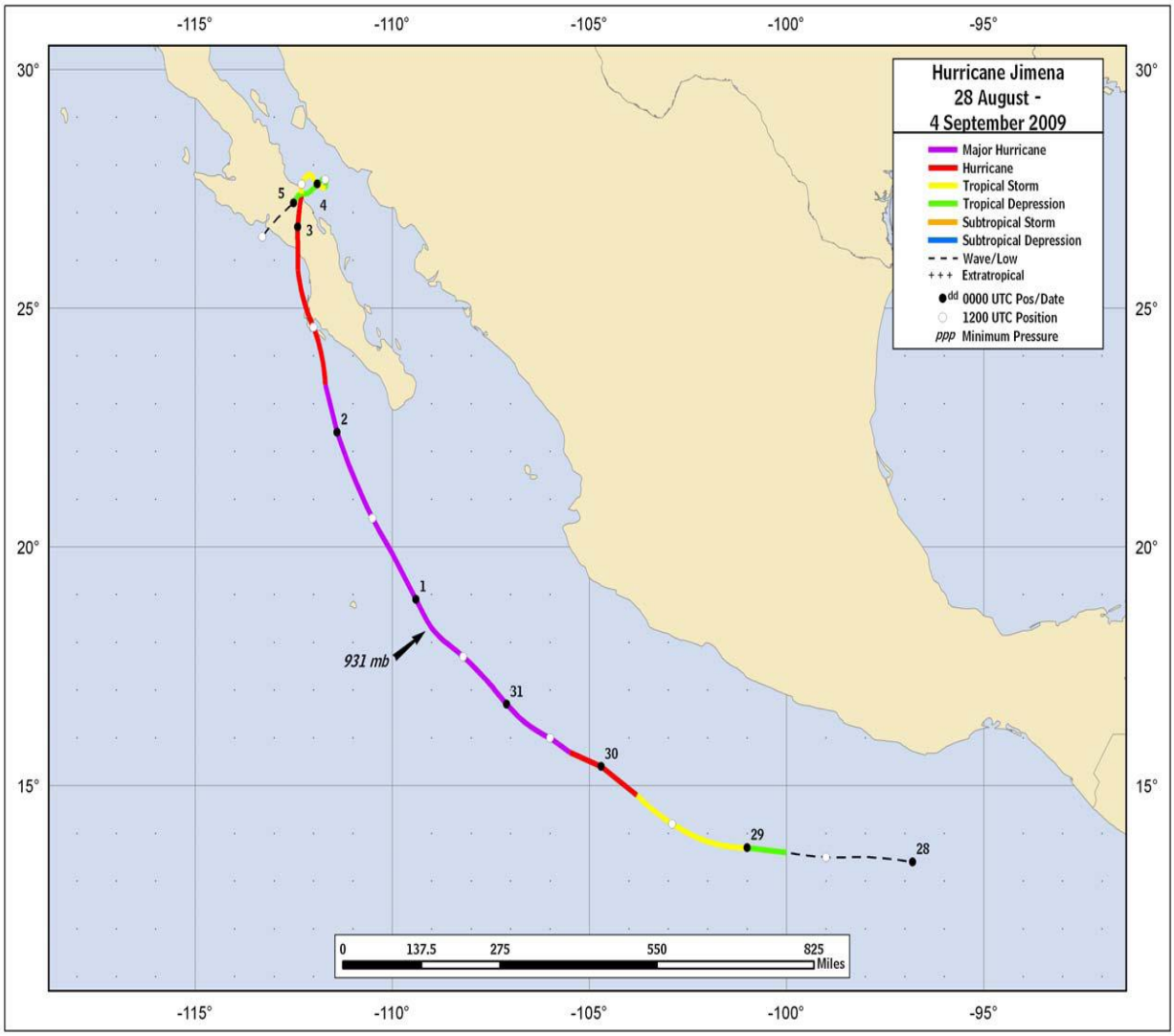

Figure 4. Best track positions for Hurricane Jimena, 28 August – 4 September 2009, Green- Tropical Depression, Yellow- Tropical Storm, Red-Hurricane, and Violet Major Hurricane, (Provided by NHC).

Table 1

Summary of NHC Best track for Hurricane Jimena, 28 August – 4 September 2009

Date/Time (UTC)	Latitude (°N)	Longitude (°W)	Pressure (mb)	Wind Speed (kt)	Stage
28/0000	13.4	96.8	1008	25	low
28/1800	13.6	100.0	1007	30	tropical depression
29/0000	13.7	101.0	1005	35	tropical storm
29/1800	14.8	103.8	980	75	hurricane
30/1800	16.3	106.6	945	120	Category 4 Hurricane
31/1900	18.3	109.0	931	135	minimum pressure
01 / 0600	19.7	109.9	933	130	TC began to weaken
02/1200	24.6	112.0	971	90	Landfall on Isla San Margarita, Baja California del Sur
02/1300	24.8	112.1	972	90	Landfall at Puerto San Carlos, Baja California del Sur
02/2100	26.3	112.4	980	75	Landfall just east of San Juanico, Baja California del Sur
03/0600	27.4	112.3	997	50	tropical storm
04/1900	27.4	112.3	1006	25	Landfall near Santa Rosalia, Baja California del Sur
05/1800					dissipated

3.3 Model Initialization

Five different datasets of NCEP FNL (Final) Operational Global Analysis, Real-Time, Global, Sea Surface Temperature (RTG_SST) analysis product, Gridded Satellite (GridSat), NCEP ADP Global Upper Air Observational Weather Data and NCEP ADP Global Surface Observational Weather Data have been used in this research.

Table 2

NHC official (OFCL) and climatology-persistence skill baseline (OCD5) track forecast errors (n mi) for Hurricane Jimena (2009)

Model	Forecast Period (h)						
	12	24	36	48	72	96	120
OFCL (Jimena)	**23.3**	**43.5**	**58.9**	**64.4**	**52.4**	**109.4**	218.8
OCD5 (Jimena)	34.0	71.5	116.8	157.0	241.0	372.2	503.4
Forecasts	26	24	22	20	16	12	8
OFCL (2004-8)	31.0	51.7	71.7	90.2	123.6	161.3	201.8
OCD5 (2004-8)	38.4	73.6	111.9	149.1	214.2	261.1	311.5

Table 3

NHC official (OFCL) and climatology-persistence skill baseline (OCD5) intensity forecast errors (kt) for Hurricane Jimena 2009

Model	Forecast Period (h)						
	12	24	36	48	72	96	120
OFCL (Jimena)	6.9	10.4	14.1	**11.5**	**12.5**	**10.0**	**8.9**
OCD5 (Jimena)	8.6	13.1	15.8	17.2	25.6	26.0	22.12
Forecasts	26	24	22	20	16	12	8
OFCL (2004- 8)	6.2	10.2	13.3	15.1	17.7	19.0	18.8
OCD5 (2004-8)	7.1	11.5	14.7	16.8	18.9	20.3	20.2

The NCEP FNL Operational Global Analysis product is provided at the surface, at 26 pressure levels ranging from 1000 mb to 10 mb, in the surface boundary layer, some sigma layers, and the tropopus. The FNL analysis is available at 6-hour interval (00, 06, 12 and 18 UTC) on 1.0 degree resolution for surface with 26 Surface pressure, sea level pressure, geopotential height, temperature, sea surface temperature, soil values, ice cover, relative humidity, u- and v- component of winds, vertical velocity are some of the variables found in FNL analysis.

RTG_SST analysis product is produced daily by National Centers for Environmental Prediction/Marine Modeling and Analysis Branch (NCEP / MMAB) on a half degree grid with a two-dimensional variational interpolation analysis of the most recent 24-hours buoy and ship data, satellite-retrieved SST data, and SST' is derived from satellite-observed sea-ice coverage. The essence of RTG analyses is for weather prediction and modeling, particularly at high resolution and short range. WRF model does not require SST however it is incorporated for updating SST during the model run when running for a long period of time. The Gridded Satellite (GridSat) data are created to facilitate use of satellite data by non-satellite experts and to help facilitate large scale processing via tools designed to process CF-compliant netCDF files.

The NCEP ADP Global Upper Air Observational Weather Data are composed of global upper air weather reports operationally collected by the National Centers for Environmental Prediction (NCEP). These include radiosondes, pibals and aircraft reports from the Global Telecommunications System (GTS), and satellite data from the National Environmental Satellite Data and Information Service (NESDIS). The reports can include pressure, geopotential height, air temperature, dewpoint temperature, wind direction and speed. Data may be available at up to 20 mandatory levels from 1000mb to 1mb, plus a few significant levels. Report intervals range

from hourly to 12 hourly. These data are the primary input to the NCEP Global Data Assimilation System (GDAS), which is used to create the NCEP Final Troposphere Analyses.

NCEP ADP Global Surface Observational Weather Data are composed of surface weather reports operationally collected by the National Centers for Environmental Prediction (NCEP). The data includes land and marine surface reports received via the Global Telecommunications System (GTS). Variables recorded in the reports include pressure, air temperature, dew point temperature, wind direction and speed. Precipitation data has been decoded for the U.S. and Canada. Report intervals range from hourly to 3 hourly. These data are the primary input to the NCEP Global Data Assimilation System (GDAS).

3.4 Model Description and Experiment Design

The model used in this study is the Advanced research Weather Research and Forecast (WRF-ARW) version 3.3. The Weather Research and Forecasting (WRF) Model is a mesoscale numerical weather prediction (NWP) system widely used for operational forecasting (the Nonhydrostatic Mesoscale Model WRF-NMM) and atmospheric research (the Advanced Research Model, WRF-ARW). The WRF ARW model is a fully compressible, nonhydrostatic model Idealized simulations (e.g. convection), regional and global applications, parameterization research, data assimilation research, forecast research, real-time NWP, hurricane research, coupled-model applications and teaching are some of examples of applications of WRF. It supersedes and is more advanced than MM5 for fine-resolution numerical weather prediction (NWP) due to its mass conservation, improved numerics and expanding physics (Deng et al. 2007).

The flowchart in Figure 5 is an illustration of the component of the WRF Modeling System version 3.3. The WRF Preprocessing System (WPS), WRF-Var, ARW solver and Post-

processing & Visualization tools constitute the major program in WRF Modeling System for the real-data case using WRF-Var. WPS consisting of three programs of geogrid, ungrib metgrid is the first step when running a real-data case using variational analysis in WRF. The geogrid program defines the simulation domains using information specified by the user and interpolates various terrestrial data sets to the model grids. The ungrib program reads GRIB files and extracts fields to the intermediate format. Output from the ungrib program is horizontally interpolated by metgrid program to simulation domains defined by the geogrid program.

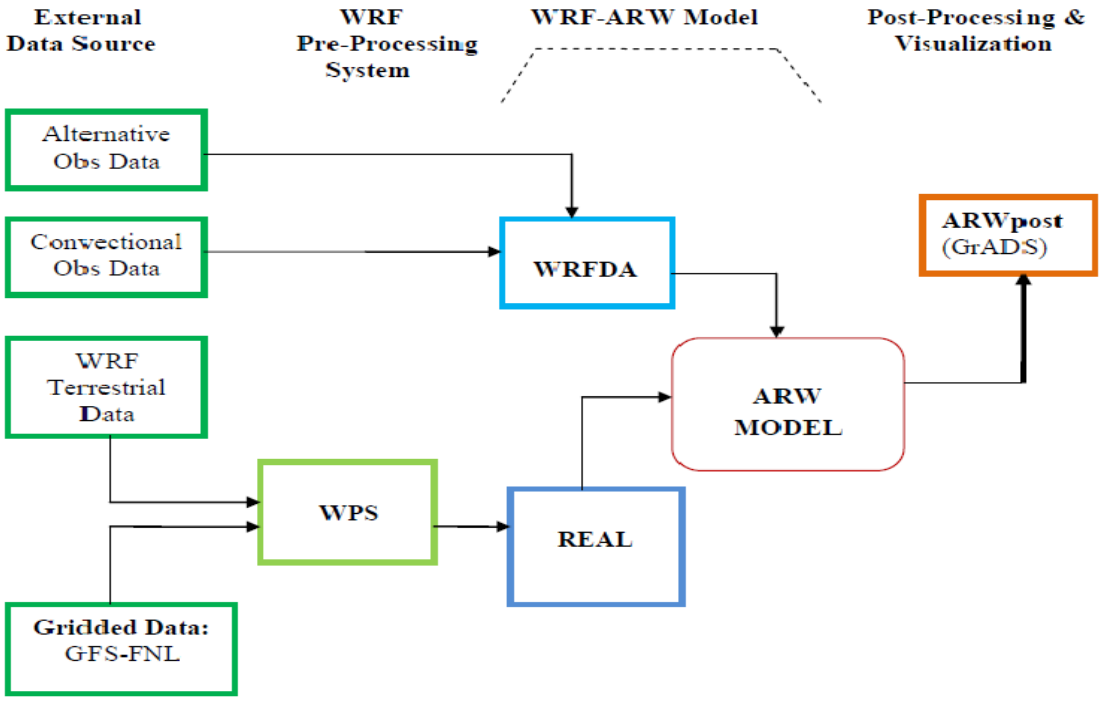

Figure 5. Flow chart of the WRF-ARW model with WRF-Var for a real-data case.

The real-data pre-processor (Real Figure 5 in blue) in the ARW generates initial and lateral boundary conditions from the interpolated metgrid output for real-data cases (Skamarock et al.2008). WRF ARW solver supports both idealized and real-data applications with various lateral boundary condition options such as periodic, symmetric, and open radiative. Recent versions of WRFDA have 3D/4D-VAR capability which can be used for variational data

assimilation. The ARW solver consists of fully compressible equation, Euler nonhydrostatic with hydrostatic available and a terrain-following, dry hydrostatic-pressure vertical coordinate. The equations governing the ARW are in flux-form with conserved mass and dry entropy (Lin et al. 2006). For the horizontal grid and time integration, the model employs Arakawa C-grid staggering and the third-order Runge-Kutta scheme respectively. Top boundary conditions use gravity wave absorbing like diffusion, Rayleigh damping, or implicit Rayleigh damping for vertical velocity with Physical or free-slip as the bottom boundary conditions. In addition, the model supports nesting (One-way, two-way and moving nest option), nudging, prognostic variables, spatial discretization (2nd- to 6th-order advection options), and turbulent mixing and Model Filters.

Finally, WRF physics option is categorized into microphysics, cumulus parameterization, planetary boundary layer (PBL), land-surface model and radiation. The development of WRF has been a collaborative partnership, principally among the National Center for Atmospheric Research (NCAR), the National Oceanic and Atmospheric Administration (the National Centers for Environmental Prediction (NCEP) and the Forecast Systems Laboratory (FSL), the Air Force Weather Agency (AFWA), the Naval Research Laboratory, the University of Oklahoma, and the Federal Aviation Administration (FAA).

In this study, Rapid Radiative Transfer Model (RRTM) and Dudhia scheme are employed for the longwave and shortwave radiation respectively. A third-order Runge-Kutta numerical scheme and Yonsei university boundary-layer option are applied. The first part of the study focuses on the impact that orography has on the cyclogenesis of Jimena. A single domain as seen in Figure 6a focuses on the disturbances moving west-ward from Gulf of Mexico and across the Mexican mountains until it became a tropical depression. This domain has a grid resolution of 30

km with a dimension of 68 by 68 grid points. Lin et al. microphysics and 34 vertical levels are applied in this case. The model is initialized on August 24 with NCEP FNL (Final) Operational Global Analysis and was run for 7 days. The second part of the research concentrates on the tracks and intensification of the storm. A two-way, nested domain configuration (Figure 6b) is used in the WRF-ARW simulation. The dimension of the parent (or outer nested) domain (d01) is 207 by 176 km grid points and that of the child (or inner nested) domain (d02) is 376 by 340. The grid resolution is 30 km by 10 km respectively with a time step of 90 s. Lin et al (2006) discovered that ARW model is sensitive to the microphysics parameterization schemes thus in order to choose a setup MP scheme for this experiment three different microphysics schemes in the ARW-WRF model are tested.

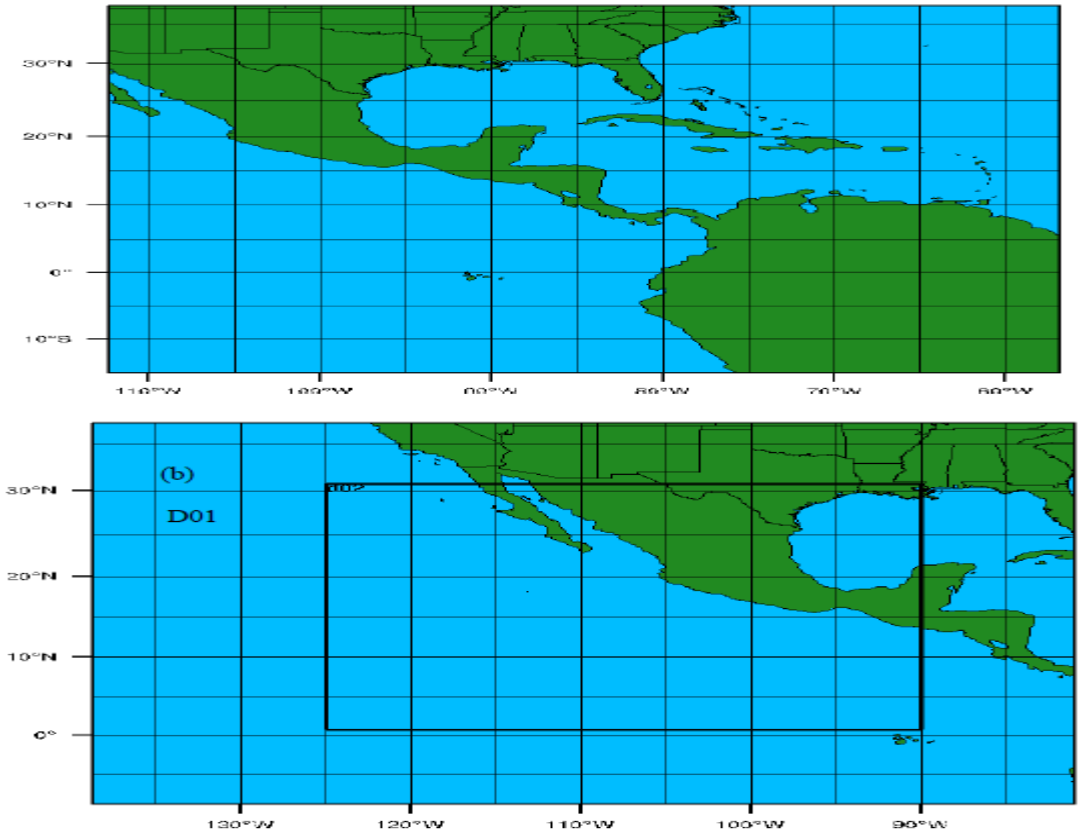

Figure 6. A single domain on 30 km resolution (a) and (b) two nested domains (30 and 10 km) plotted with plotgrids.ncl.

The experimented microphysics schemes are Purdue Lin et al. scheme (Chen and Sun 2002), WRF Single-moment 6-Class Microphysics (WSM 6) scheme (Hong *et al*. 2002) and Thompson graupel scheme. In addition, three different starting time - August 25, August 27 and August 28 are carried out to in order to examine the impact of initial conditions on FNL data. The control experiment is performed with the same setup described in case 2 but with Lin et al scheme as microphysics and integrated from 28 August 00Z to 5 September 00Z 2009. Another experiment is conducted using the WRFDA.

CHAPTER 4

Three-Dimensional Variational (3DVAR) Data Assimilation

4.1 Initial conditions

According to Lin (2007) numerical weather predication (NWP) can be viewed as solving an initial-boundary value problem whereby the governing equations of geophysical fluid system are integrated forward in time in a finite region and in addition to suitable initial conditions required for the model. Thus given an estimate of the current state of the atmosphere (initial conditions), and appropriate surface (e.g. the atmosphere or the ocean), boundary condition, the model simulates or forecast the atmospheric evolution (Eugenia Kalnay, 2003). The ability of NWP model to efficiently forecast depends on the resolution of the model and the accuracy of dynamical and physical processes as well as initial conditions used to initialize the model (Holton, 2004). Despite availability of all sources of data (such as radiosonde, surface, dropsonde data, sodars, radars, satellite etc), errors in observational data are inevitable due to the fact that observations are sparse in some of the regions, incomplete, and irregularly distributed in time and space (Wang et al, 2000). It is therefore necessary to provide numerical weather prediction with high quality and accurate estimate of the initial conditions; data assimilation aims to decrease errors in initial conditions of numerical weather prediction models. Beside the uncertainties in observation, NWP model solutions may generate noise such as sound, gravity waves etc. The presence of gravity waves is an indication that temperature and pressure are unbalanced, thus this may lead to unreasonable forecast. The gravity waves can be eliminated by analyzing the model initial conditions using DA. Data assimilation plays a vital role in the studies of atmospheric, oceanic problems and numerous applications in NWP due to its capability to improve forecasting or modeling (Wang et al, 2000).

Data assimilation is the process whereby observational data is incorporated into a NWP model to obtain suitable set of data to initialize a model (Holton 2004). In other words DA produce a better estimate (the analysis) of the atmospheric condition using observations, or previous forecasts and their respective error statistics which is then used as initial condition for numerical weather initialization (Barker et al). Bouttier et al. (1999) categorized data assimilation into two basic approaches: sequential and non- sequential assimilation. Whiles the non-sequential assimilation may use observation from the future, for instance in a reanalysis exercise assimilation, the sequential assimilation only considers observation made in the past until the time of analysis, like the case of real-time assimilation systems (e.g. 3D-Var nudging optimal Interpolation (OI), etc). Variational data assimilation consists of 3D-Var and 4D-Var and was developed to replace previously used schemes example Cressman (MM5), Newtonian nudging (FDDA – MM5) and optimum interpolation (OI). The basic goal of a variational approach is to produce an "optimal" estimate of the model initial state from a combination of observations and prior NWP. (Ide et al. 1997). Barker et al. (2003) listed the following as the practical advantages of variational approach over the OI:

- Observations can easily be assimilated directly without the need for prior retrieval. This results in a consistent treatment of all observations and, as the observation errors are less correlated (with each other and the background errors), practical simplifications to the analysis algorithm.
- The VAR solution is found using all observations simultaneously, unlike the OI technique for which a data selection into artificial sub-domains is required.

4.2Three-dimensional variational assimilation (3DVar)

Three-dimensional Variational Data Assimilation system was initially built to run on

MM5 but can now be used for initialization of WRF (Michalakes et al., 2001). WRF Variational Data Assimilation (WRF-Var) system which supports 3DVAR and 4DVAR capability currently is being maintained and supported by the Mesoscale and Microscale Meteorology Division of NCAR. Observations are processed in small batches (intermittent technique) with the three-dimensional Variational Data Assimilation. According to Navon (2009), the cost function of 3DVAR is proportional to the square of the distance between analysis and both background and observations. Mathematically, he defines cost functional J(x) of WRF 3DVAR scheme is as:

$$J(X') = 1/2 \{ [y^o - H(x)]^T R^{-1} [y^o - H(x)] + (x-x^b)^T B^{-1} (x-x^b)\}$$

$$B = (x^b - x^t)(x^b - x^t)^T = (\varepsilon^b \varepsilon^b)^T$$

$$\approx (x^{T+24} - x^{T+12}) (x^{T+24} - x^{T+12})^T$$

$$x = x^b + W [y^o - H(x^b)]$$

where **B** is the background error covariance, ***R*** is the observation error covariance, ***H*** is an interpolation operator (or observation operator), x^b is the first guess or background, y^o is the observation, $y^o - H(x^b)$ are the observational increments, $x = x^a$ is the analysis, x^t is the true atmospheric state, ε^b is the background error, *W* is a weight matrix based on statistical error covariance's of forecast and observations. $1/2 [y^o - H(x)]^T R^{-1} [y^o - H(x)]$ measure the distance of forecast field *x* to observations y^o and $(x-x^b)^T B^{-1} (x-x^b)$ measures the distance to background x^b.

Figure 7 is a flow diagram of WRF model with the blue rectangle representing the main component of WRF-3DVAR scheme. Background Preprocessing, Observation Preprocessor and Background Error Calculation produce input first guess (x^b), observation (y^o) and background error respectively for WRFDA. The output analyses (x^a) is used as the initial conditions and for

the WRF simulation and the lateral boundary conditions are then modify to reflect the differences between background forecast and analysis.

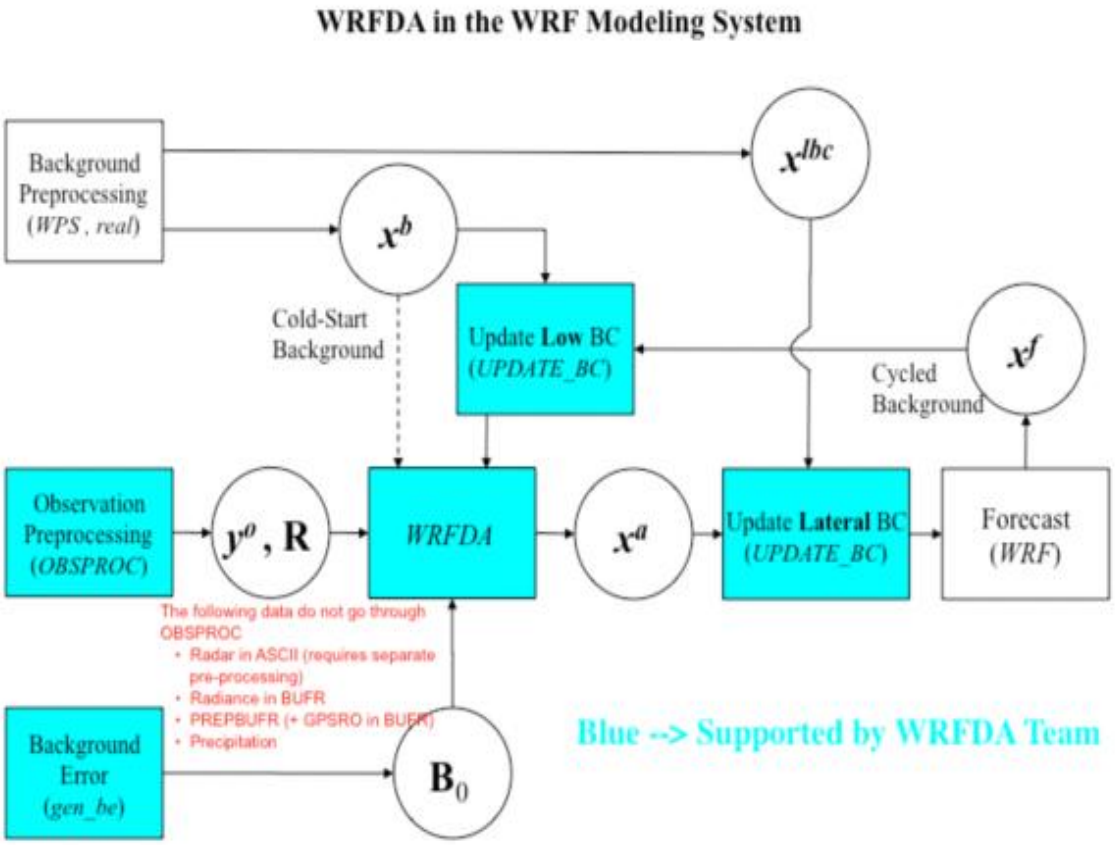

Figure 7. Flow Chart of WRF Modeling.

x^b first guess, either from a previous WRF forecast or from WPS/REAL output.

x^{lbc} lateral boundary from WPS/REAL output.

x^a analysis from the WRFDA data assimilation system.

x^f WRF forecast output.

y^o observations processed by OBSPROC. (note: PREPBUFR input, radar, radiance, and rainfall data don't go through OBSPROC).

CHAPTER 5

Results and Discussion

This study is to investigate the orographic influence on the genesis of tropical cyclones and its association with AEW-MCS in the North Eastern Pacific Ocean using data assimilation. In this chapter, we examine the system that later become Jimena after it entered into the Eastern pacific on August 28 using the University of Wisconsin - Madison Cooperative Institute for Meteorological Satellite Studies (UW-CIMSS) and NCEP FNL analysis data. Result of Hurricane Jimena from the control experiment is discussed and compared to the Gridded Satellite (GridSat) data, the National Hurricane Center (NHC) best track, and the NCEP FNL analysis data. Next, the results from the sensitivity experiments with the data assimilation are presented and compared to that of the control experiment.

5.1 Tracking Pre-Jimena

Appendix B (Table 28 & 29) shows Brightness Temperature of cloud top temperature (a proxy for AEW/MCS) of pre-Jimena from 8/23/18Z to 8/28/18Z on the right panel and cloud top temperature for Hurricane Jimena from 8/29/06Z to 9/03/06Z on the left panel derived from the Gridded Satellite. The storm was manually tracked back to off the coast West Africa near 30^{o}W. Note that cloud top temperature associated with the AEW become cold as it travels west and much colder as it approaches the mountain ranges of Mexico. Also using the positive Relative Vorticity plot from University of Wisconsin-Madison Cooperative Institute for Meteorological Satellite Studies (UW-CIMSS) in Appendix C (Figure 30 to 34) we were able to trace system back to the tropical Atlantic near the coast of West Africa. The dash lines show the track of the TC and the tropical waves that triggered it. Figure 8 is a plot of positive relative vorticity at 500-mb as a function of time and longitude of u-wind and v-wind averaged between 8° N and 18° N

using NCEP FNL analysis data panel (a) and panel (b) is hovmöller plot of brightness temperature using Gridded Satellite data. Note that both FNL analysis plot compare very well in terms of track with brightness temperature plot. In both plot we observed the AEW and its related MCS moved along Intertropical Convergence Zones (ITCZ) before it became a tropical cyclone on August 28. The red arrow in 8a shows that the relative vorticity decreased on August 24 before the system passed over the Central American Mountains and the maximum relative

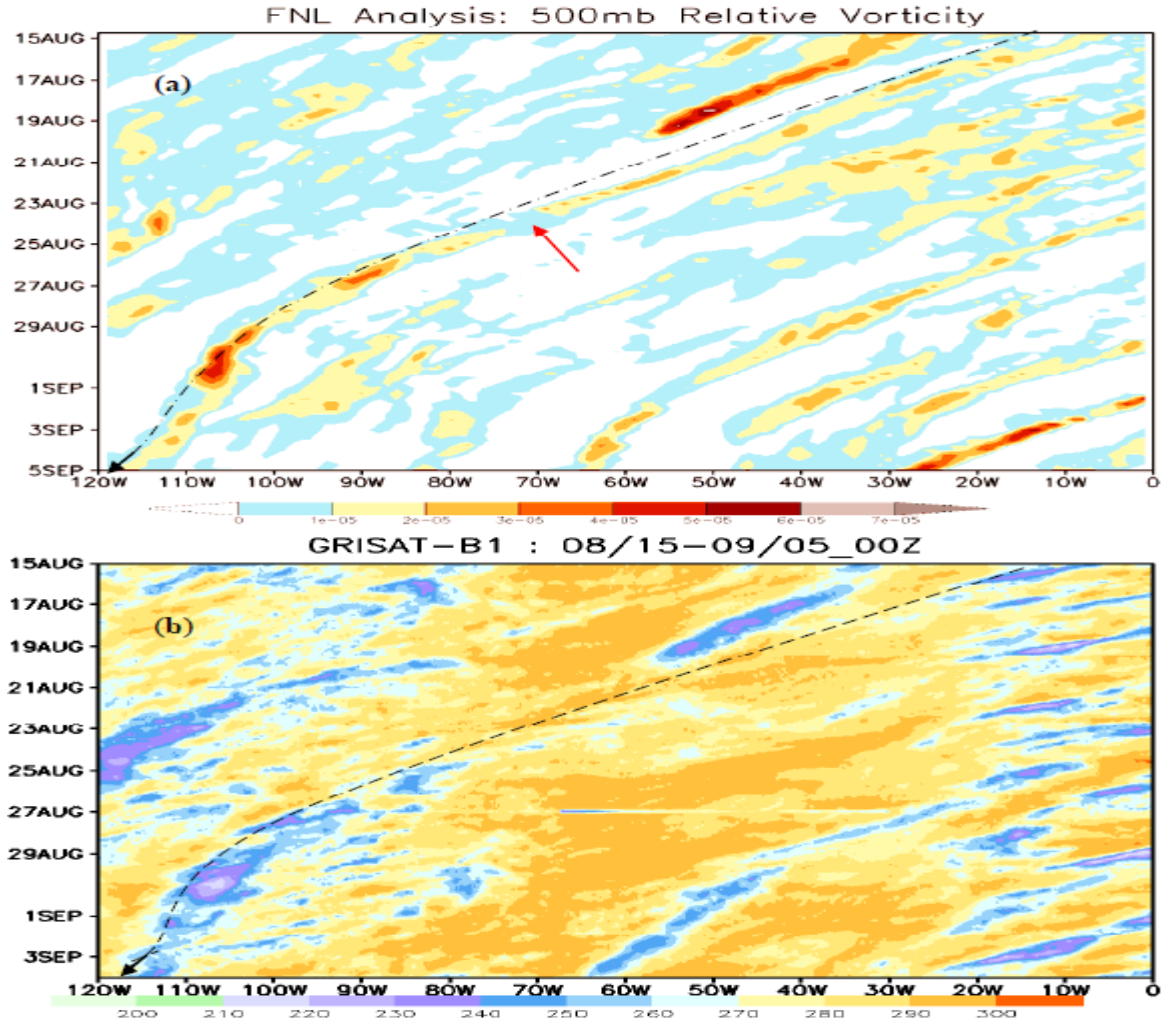

Figure 8. (a) Hovmöller diagram of positive relative vorticity (ms^{-1}) in shaded contour areas for NCEP FNL analysis data at 500 mb averaged between 8° N and 18° N for 00Z 15 August to 00Z 05 September. (b) Brightness Temperature using gridded Satellite data.

vorticity occurred three days after it developed into a tropical cyclone. The dashed curve in the diagram traces Jimena back to 5 degrees W thus associating AEWS-MCS with the formation of Eastern Pacific hurricanes.

The relative vorticity hovmöller diagram also shows increase in vorticity in two areas on August 27 and August 31 indicating rising motion and powerful thunderstorm activities. Observe that temperature were below 220-K between 100^{o}W and 110^{o}W indicating thunderstorms around the center of the storm lower sea level pressure occurred after the wave entered pacific basin with a minimum sea level pressure of 998 mb on (Figure 8.b).

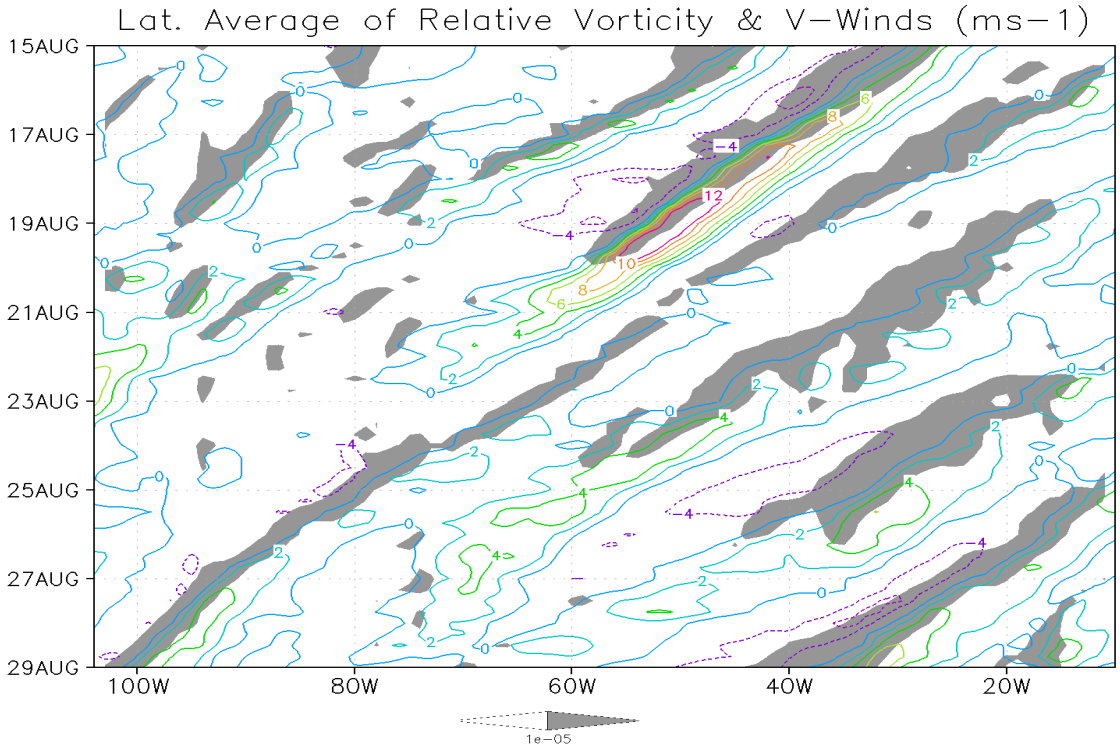

Figure 9. The NCEP reanalysis plot of 700mb to 500mb average Relative Vorticity (values equal or greater than $1x10^{-5}$ s^{-1} are shaded) and V-winds (contour) between 8°N and 18°N latitude.

Figure 9 represents Hovmöller diagram of 700 to 500-mb averaged between 8°N and 18°N degrees north latitude of relative vorticity and meridional winds (V-winds) with maximum v-winds are 13 ms^{-1}. The diagram shows a cyclonic activity over the Atlantic Ocean

approximately at 15ºW on August 16. In Figure 11 using WRF simulated Relative Vorticity averaged between 1000mb-700mb we were able to track the storm back to the Gulf of Mexico. A low cyclonic system can be seen at the beginning of the simulation with relative velocity of 5 x 10^{-5}. This is the disturbance that later triggered Hurricane Jimena on August 28. An area of high relative vorticity maximum of 0.00035 ms^{-1} occurred between 90W and 100 probably as a result orographic effect.

Zonal cross section of the mean zonal wind for 08/15/00Z to 09/05/00Z is shown in Figure 10. The strongest wind is found near 10^{o}W at 900 mbar with velocity around $5ms^{-1.}$

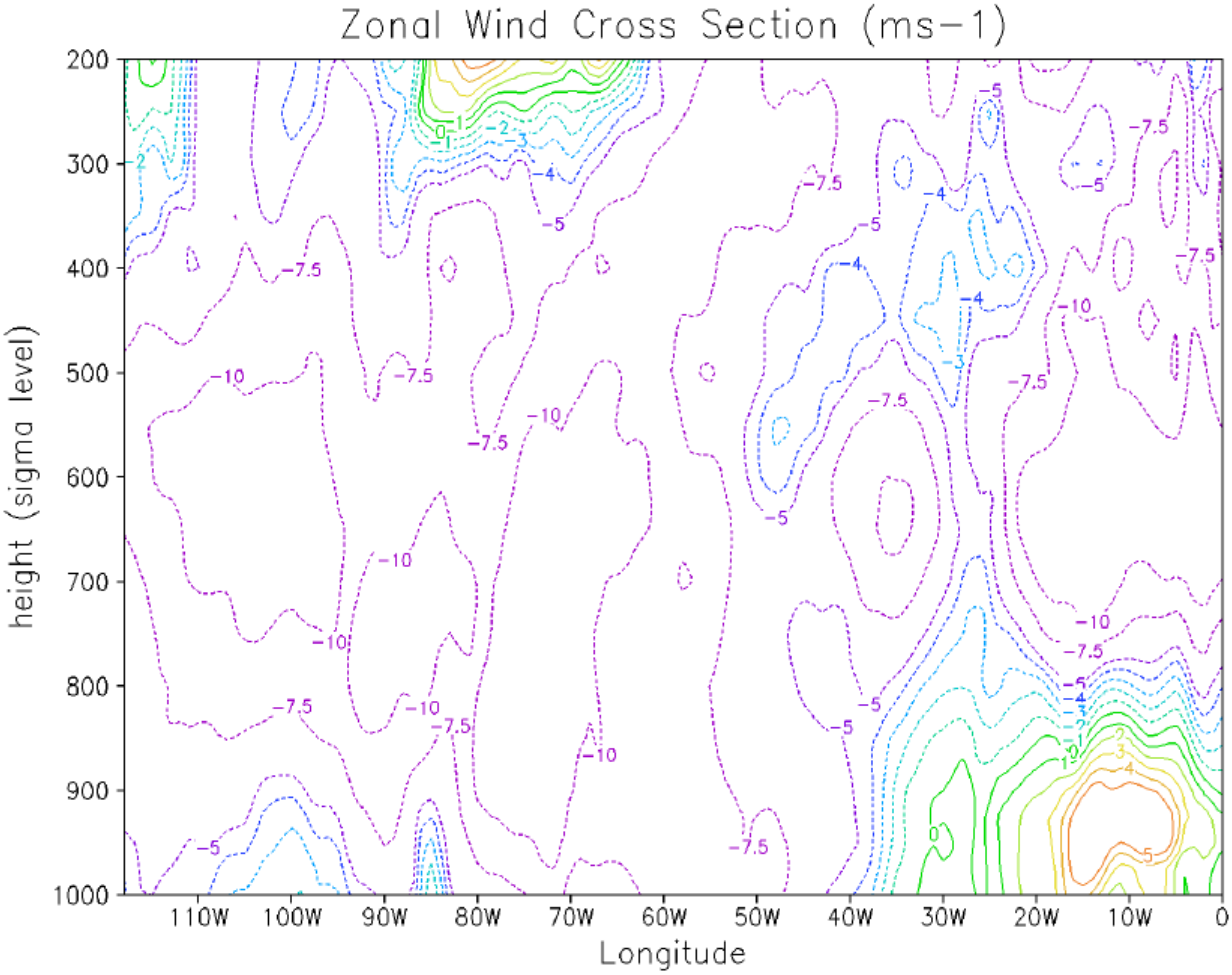

Figure 10. The NCEP reanalysis zonal winds cross section for which latitude is average between 8°N and 18°N for N for 00Z 15 August to 00Z 05 September.

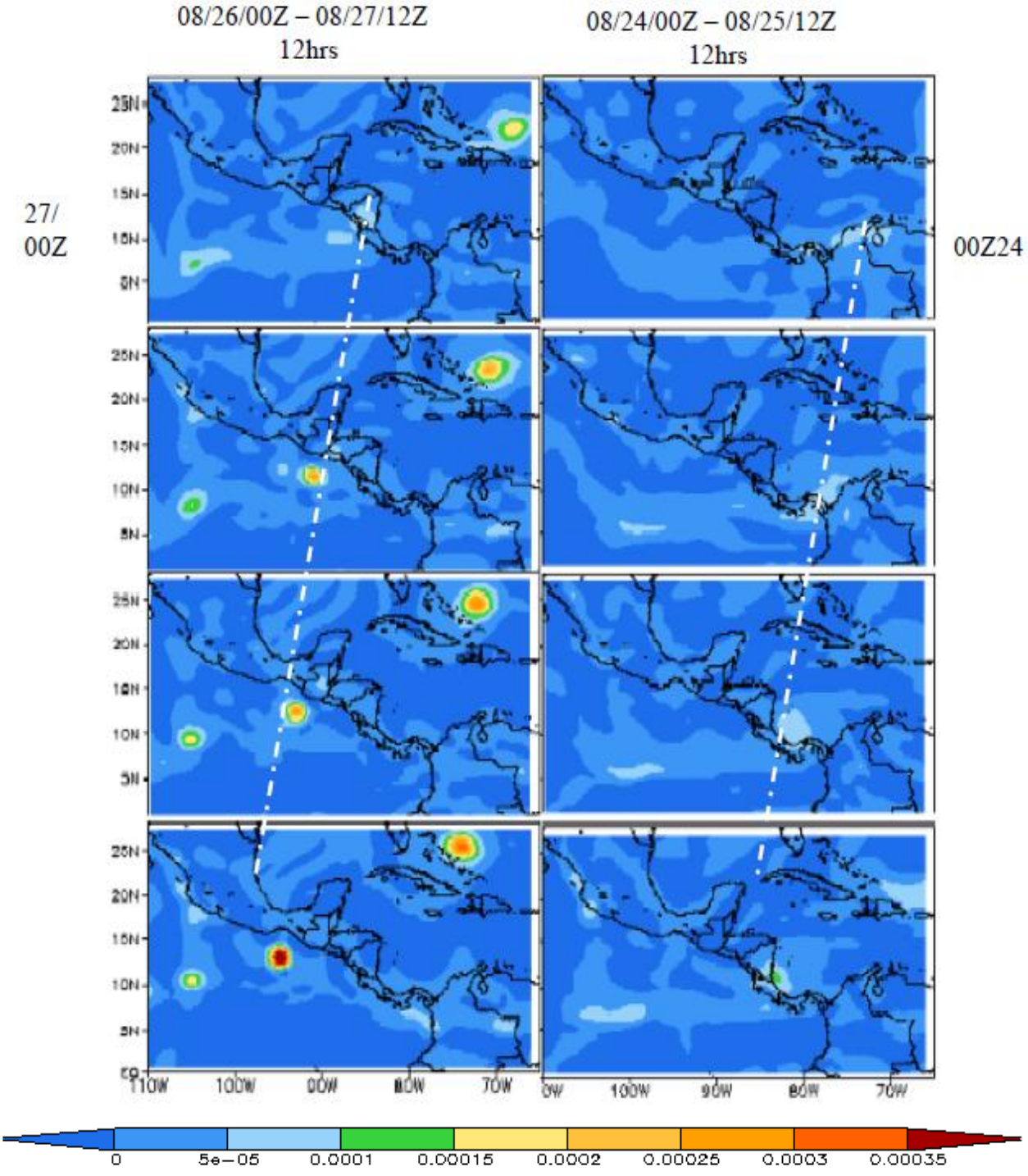

Figure 11. WRF simulated Relative Vorticity at 00Z and 12Z from 8/24/ to 8/27 for every 12hrs (averaged between 1000mb-700mb) with Maximum Relative Vorticity is 0.00035 ms-1 and minimum at -10e-05 ms-1.

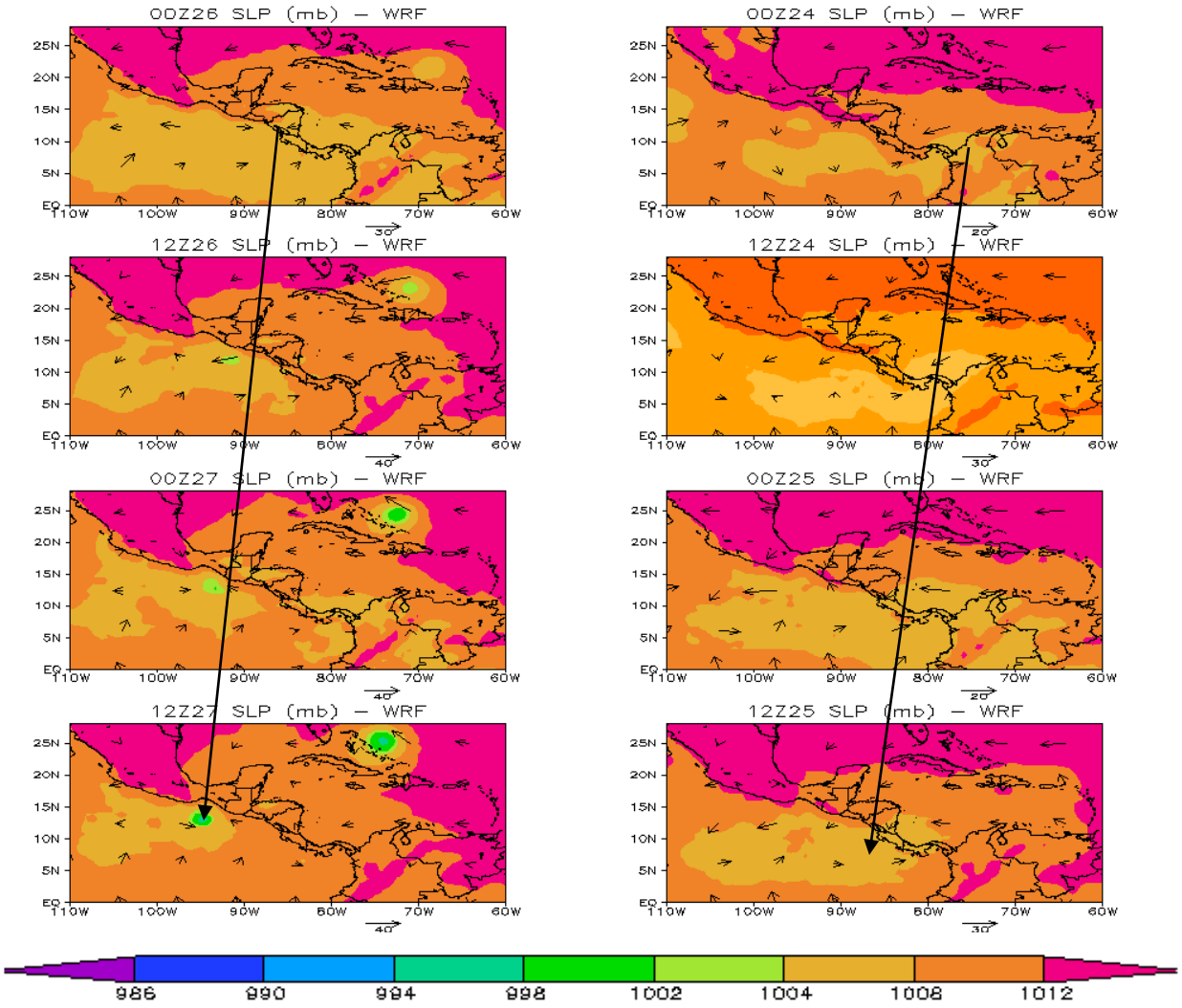

Figure 12. Shaded contours are min Sea Level Pressure (mb) and vectors represent surface wind speed from 8/24/00Z to 8/27/12Z for every 12hrs.

Figure 12 is a plot of minimum sea level pressure mbar *(*contour) and surface wind (vector) for WRF-ARW experiments from 8/24/00Z to 8/27/12Z for every 12hrs. The minimum sea level pressure of the disturbance from August 24 00Z to August 26 00Z was about 1008 mb for the stimulated storm. The pressure of the system however began to decrease from August 26/12Z to August 27/12Z. Figure 13 shows u10 wind (m/s) of the WRF-ARW simulation. The maximum surface wind speed of the precursor at the beginning of the simulation was approximately 12 ms^{-1}. Due to the orography effect the wind speed decreased from 12 m/s to less

than 9 m/s after the disturbance moved passed Central American Mountains from August 26 to the end of the simulation. Observe that system became disorganized shortly after it crossed the mountain ranges on 25th of August at 12Z.

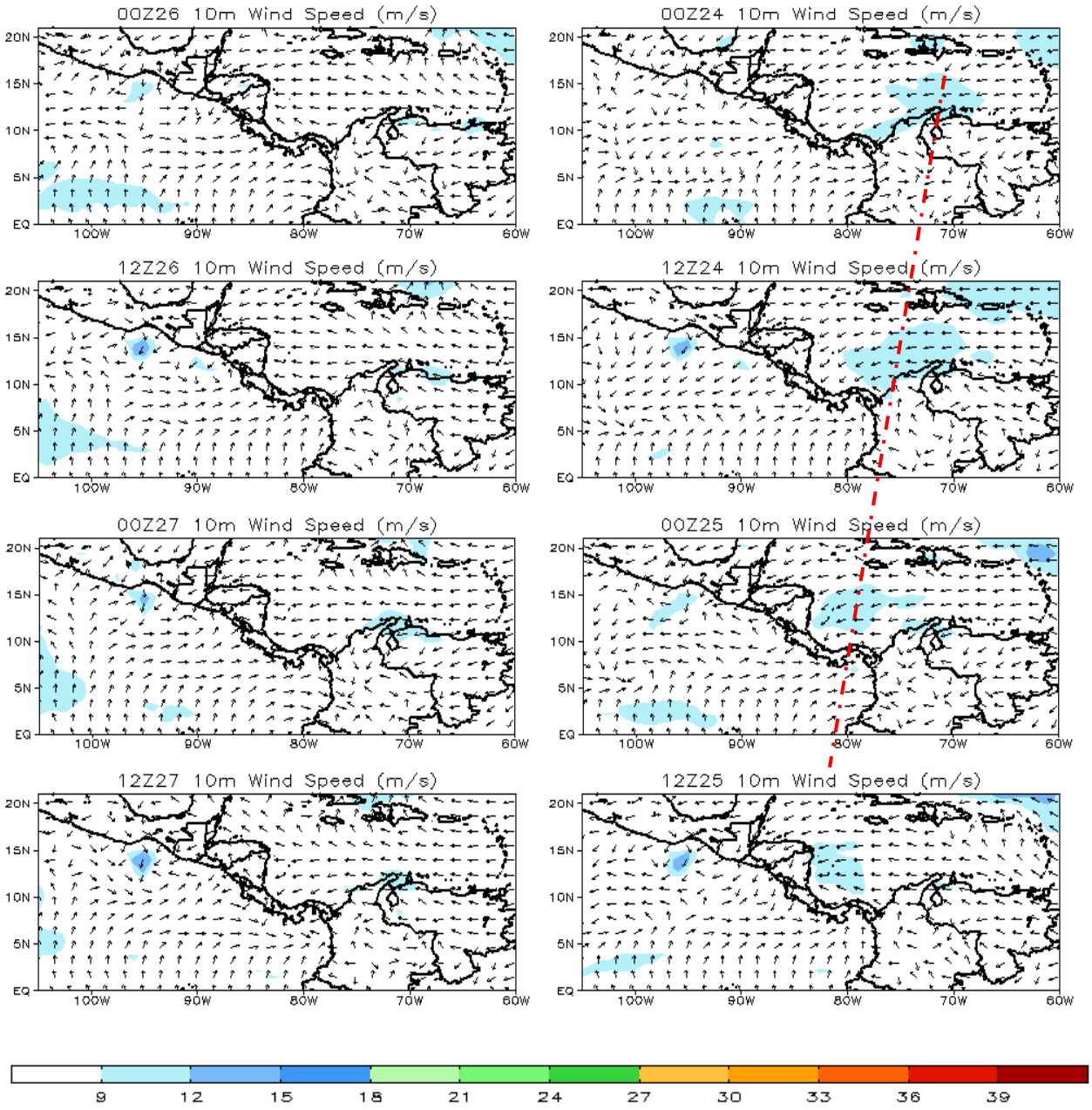

Figure 13. Shaded contours wind magnitude and solid contour wind vector from 8/24/00Z to 8/27/12Z for every 12hrs.

5.2 Control Experiment Setup

In order to setup a suitable control experiment to investigate the role that the Central America and Mexico Mountains play on tropical cyclones development and its relationship with tropical wave activities in the northeast Pacific basin, WRF simulation results from three different initial conditions and three different microphysics are discussed in this section.

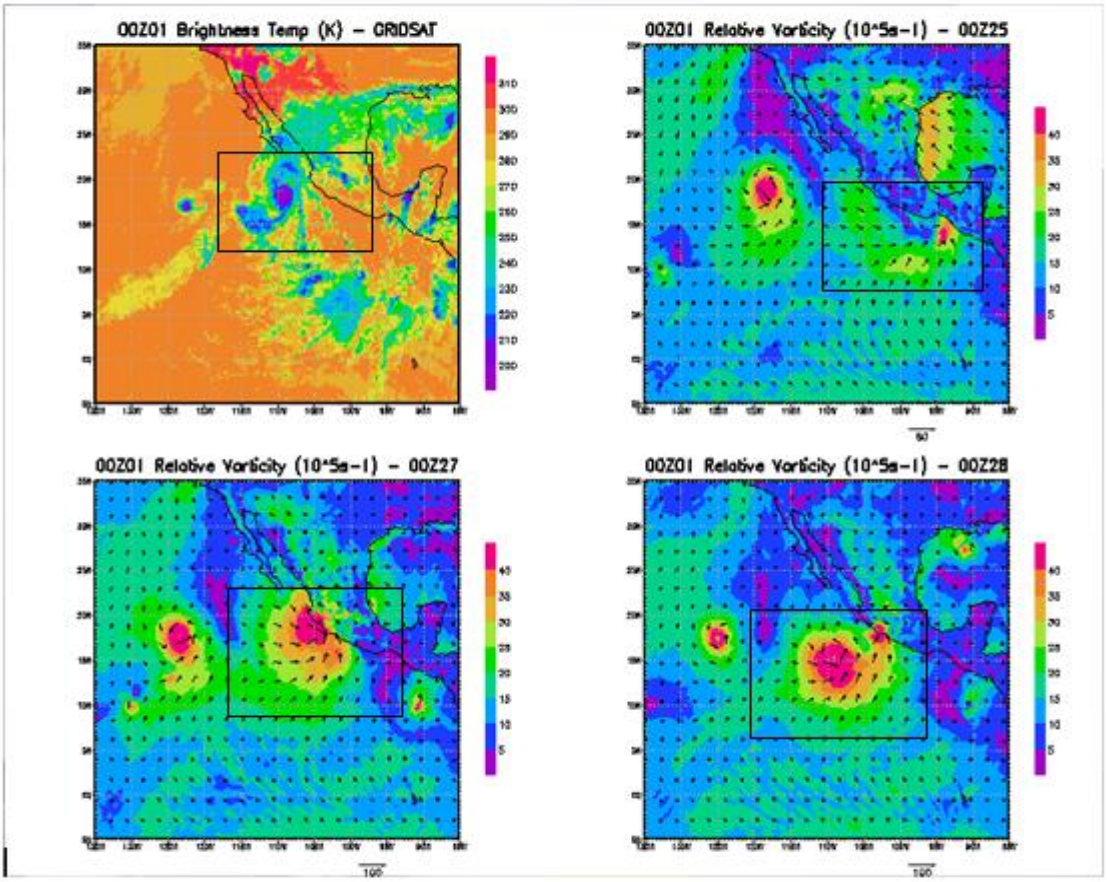

Figure 14. Sketch of brightness temperature using Gridded Satellite (GridSat) top left and stimulated Relative Vorticity on 01/09/00Z, top right, bottom left, bottom right, initialized on 25/00Z, 27/00Z, and 28/00Z respectively.

5.2.1 Sensitivity to Initial Condition. The area enclosed in the rectangle in Figure 14 shows position of hurricane Jimena on 01/09/00Z with maximum vorticity of 40 ms^{-1}. It is noticeable from Figure 14 that the position of the center of the circulation of the storm that was

initialized on 28/00Z is constantans with the observed Gridded Satellite (GridSat) image (brightness temperature). However the position of the TC simulated on 27/00Z and 28/00Z are off track compared to the observed track. Observed Jimena had already made landfall on 25/00Z and outer band of the circulation had also made landfall on 27/00Z on September 1.

Again Figure 15 shows the position of the storm simulated on 28/00Z did better than that of 27/00Z. We observed that the storm Figure 15(c) is far ahead and shifted to north-west which placed it closer to land compared to that of Figure 15(d).

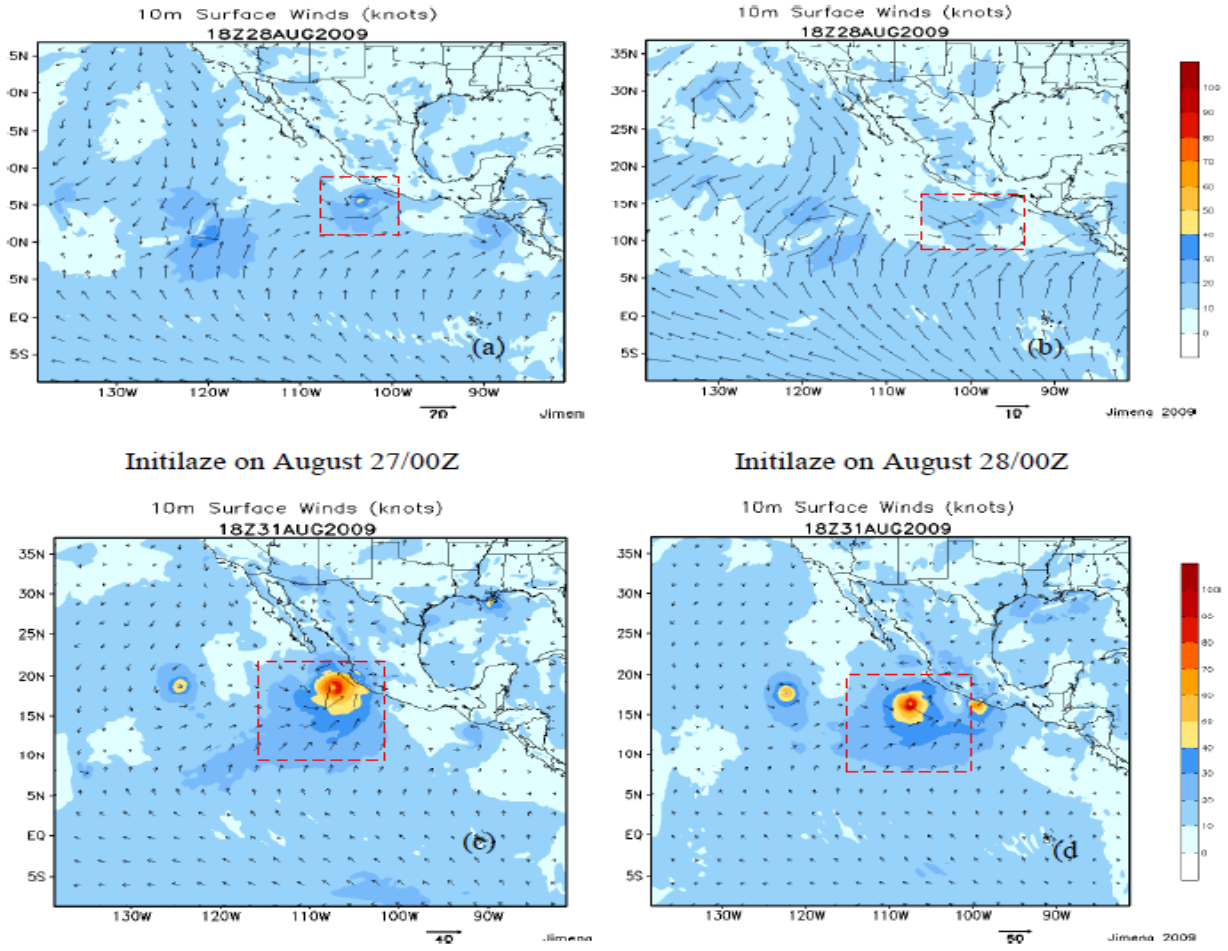

Figure 15. Simulated 10m surface winds (knot) for August 28/00z and 31 00Z Diagram (a) and (c) were initialized on 8/27/00Z, (b) and (d) initial on 8/28/00Z with maximum wind speed of 100-kt.

Moreover the propagating speed of Hurricane Jimena was about 25 kt (tropical depression, see Table 5) on 28/08/18Z however the maximum wind speed for the stimulated storm that was started on 27/00Z is approximately about 40 kt (tropical storm, see Figure 15a).

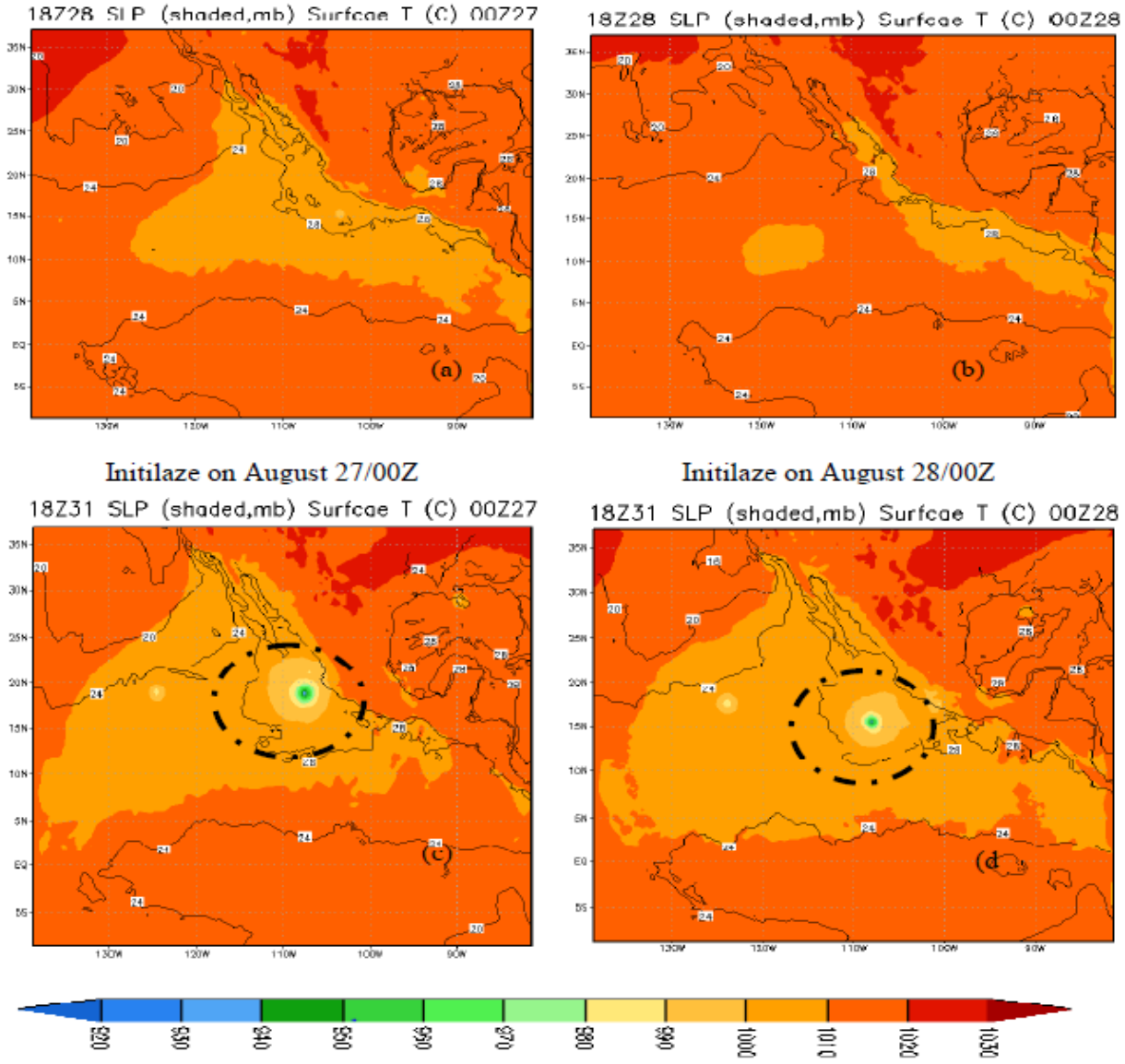

Figure 16. Comparison of Simulated Sea Level Pressure shaded (mb) and Surface Temperature in degree Celsius for 8/28/18Z and 8/30/18Z. Left column was initialize on August 27 00Z (a, c) and right column initialized on August 28 00Z (b, d). Results are based on the 30-km resolution simulation.

Figure 16 gives a comparison of the surface temperature of the simulation initialized on 27/00Z with that of the simulation initialized 28/00Z. The surface temperatures remain the same for all the cases but just like the previous plot the storm of the 27/00Z is leading and closer to land compare to 28/00Z. No evidence of significant difference between the two plot based on the sea level pressure.

5.2.2 Sensitivity to Microphysics (MP). Figure 17 compares the maximum wind speed (in m/s) obtained from observation with that of each of the three simulations using three different microphysics within the WRF model, WSM-6, Lin et al and Thompson. The result from each of the three simulated systems compares well with the observed wind speed; however the result from Lin et al scheme was the best among the three with maximum sustain wind speed of 106knot per seconds. All the three stimulated storms over predicted the intensity from 02/06Z to 02/18Z and after 04/12Z. The difference between the propagated speed of the observed and the stimulated storm averagely was about 23.4 knot. Similarly comparing the simulated track, the result shows that the Lin et al scheme did slightly better when compared to WSM 6 and Thompson schemes (see Figure 18). Observe that the storm track for all three tested microphysics, WSM, LIN, and Thompson started almost at the same location about 123 km north of the observed track (see Table 7). Thompson went further to the north and WSM-6 deviated a little bit to the south with respect to the observed in between 95^{o}W and 100^{o}W. The Lin et al. microphysics however stayed closer to the observed track from 29/00Z to 01/00Z with exception to 8/31/00Z. The WSM-6 never made a landfall and Thompson further to the west about 478 km from the observed track during landfall. Prior to landfall the cyclone's center simulation with WSM-6 microphysics was the closest. The WRF simulation using the Lin et al microphysics shows that the storm hits land approximately about 478 kilometers north east of the

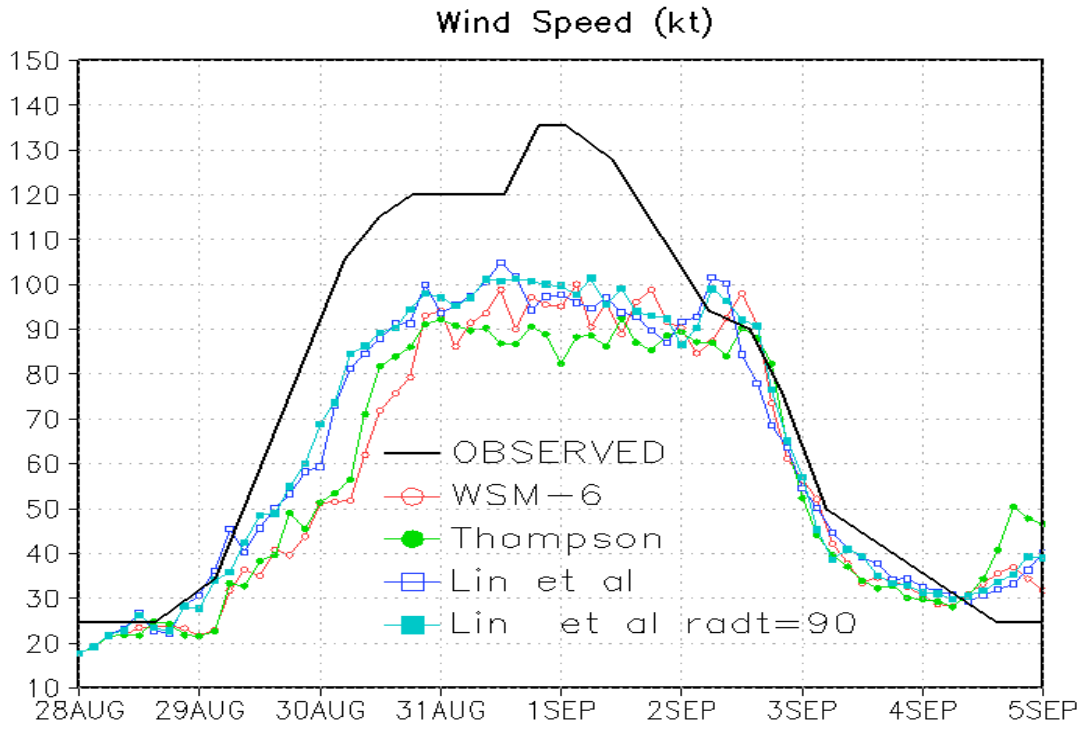

Figure 17. Observed and simulated 10m wind speed (m/s) to test the best microphysics for this study.

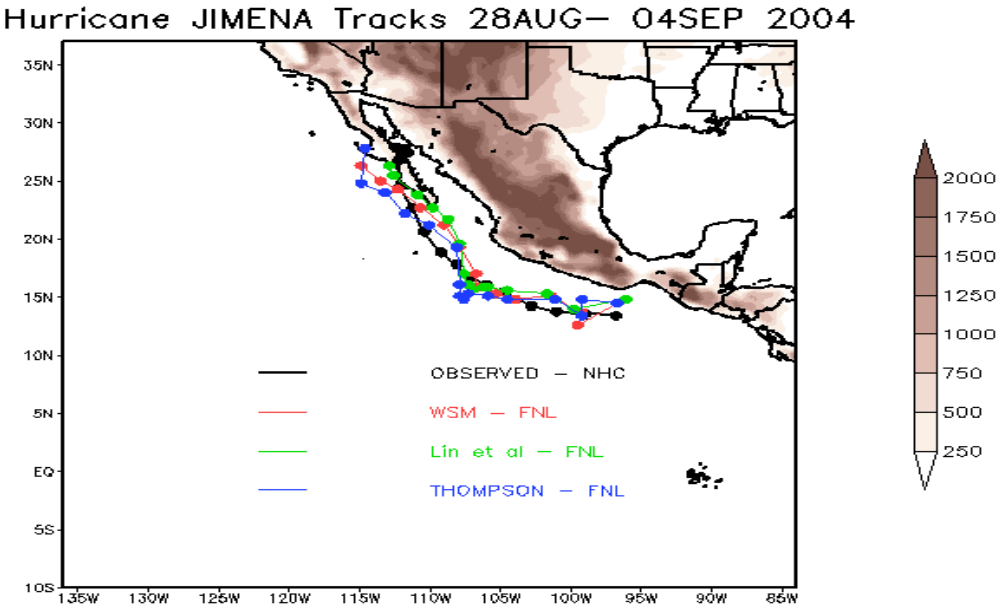

Figure 18. Unisys "Best track" and simulated tracks Solid contour to test the best microphysics for this study.

best track. The average the distance of the stimulated storm from the observed was 284 km.

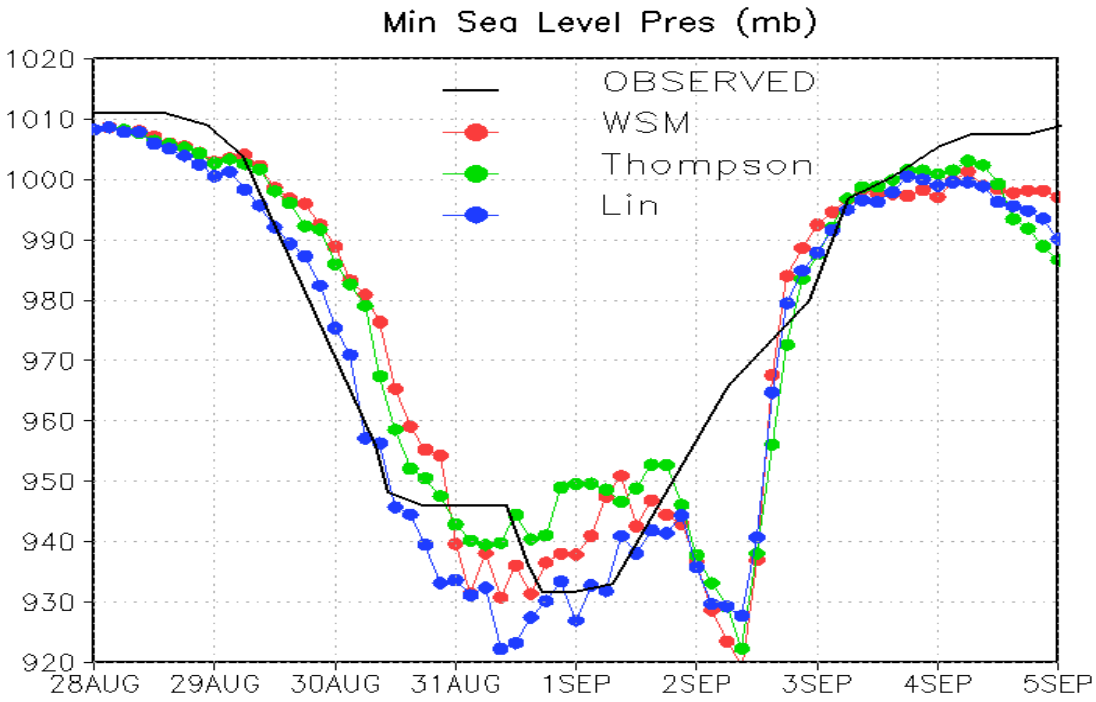

Figure 19. Minimum sea level pressures of the observation and the sensitive experiments (mb). The result is based on the 30-km resolution.

Figure 19 illustrates the minimum sea level pressure for the observation and the three tested microphysics (WSM, LIN, and Thompson). WSM-6 and Thompson microphysics produced the same sea level pressure about 1007 mb and LIN has minimum sea level pressure about 1006 mb at the start of the stimulation. The pressure for the three WRF-ARW simulations averagely was about 1 mbar lower than the observed track. The pressure for all the three cases continue to decrease and slightly drop passed the observed till 29/08/12Z. The minimum sea level pressure for WRF-ARW stimulation kept on decreasing afterwards as the storm intensifies however slightly higher than the best track. The test produced the lowest minimum slp on 09/02/12Z about 920 mb, which far lower than that of the observed (971 mb). The Lin et al. mp performed better compared to the two other microphysics.

5.3 Control Experiment

Figure 20 is sketch of sea surface temperature (F) top left, top right; relative humidity (%), bottom left and right are dew point (F) and mean sea level pressure respectively for the control experiment. The Simulated 10 meter wind speed in mph from August 28 to September 5 is represented by Figure 21. The vortex of the cyclone on August 28 at 00Z has wind speed of about 4 mph. The wind intensity kept on increasing from August 28/18Z to August 31/18Z where it attains maximum wind speed approximately 50 mph. This compares very well with the NHC's best track maximum sustained surface wind speed curve for Hurricane Jimena, 28 August – 4

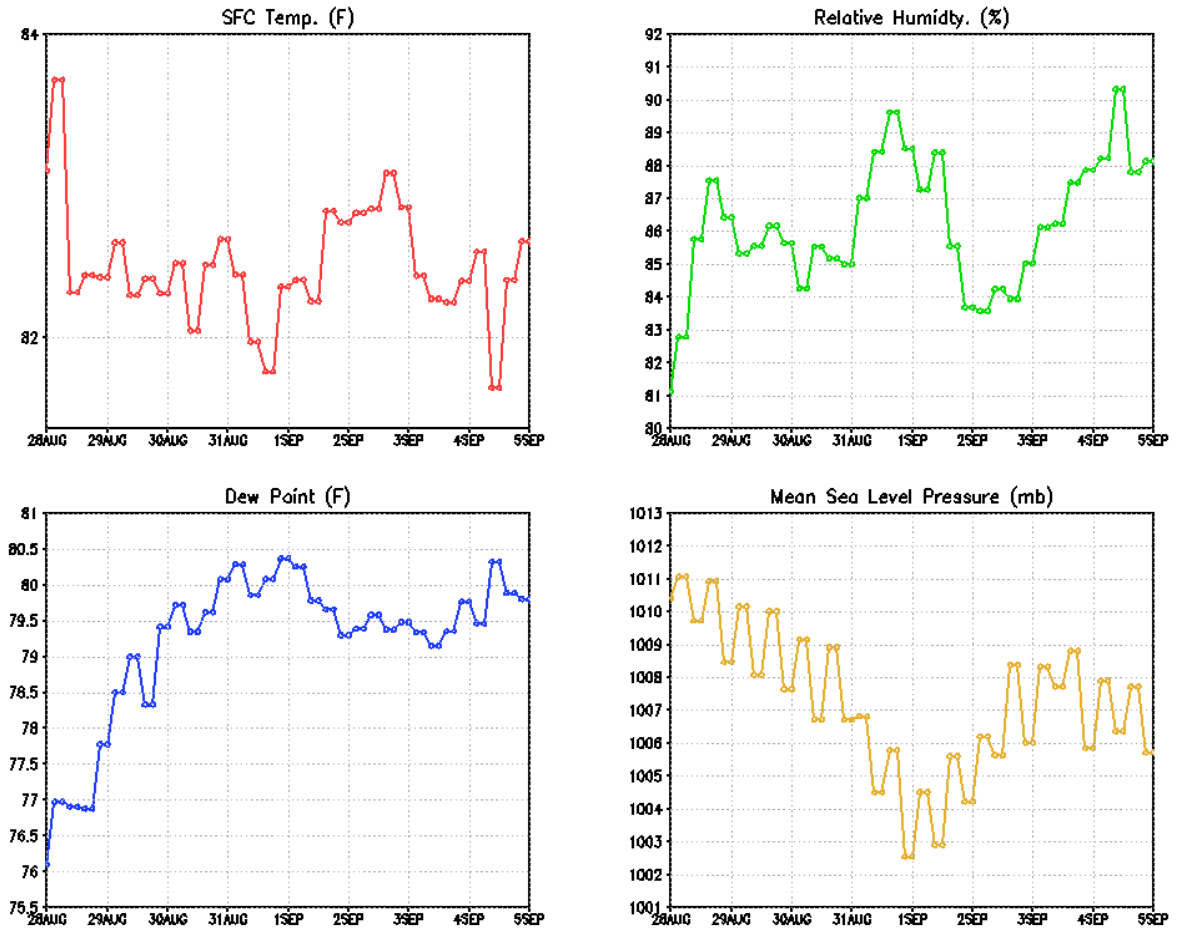

Figure 20. Sketch of Sea Surface Temperature (F) top left, top right; Relative Humidity (%), bottom left and right Dew point (F) and Mean Sea Level Pressure respectively.

September 2009 (see Appendix D, Figure 36).

According to the NHC thunder activities increased from August 27, as evident in Figure 22 which shows amount of rainfall kept on increasing throughout the period between August 28 and September 5. The simulated wind intensities are weaker compared to the observed wind intensity shown in Figure 23. The maximum of the observed wind intensity is 135 mph while that of the simulated is 105 mph. Both the control and experiments have smaller error; however the error was much higher at end of the simulation compared to that of the observed data.

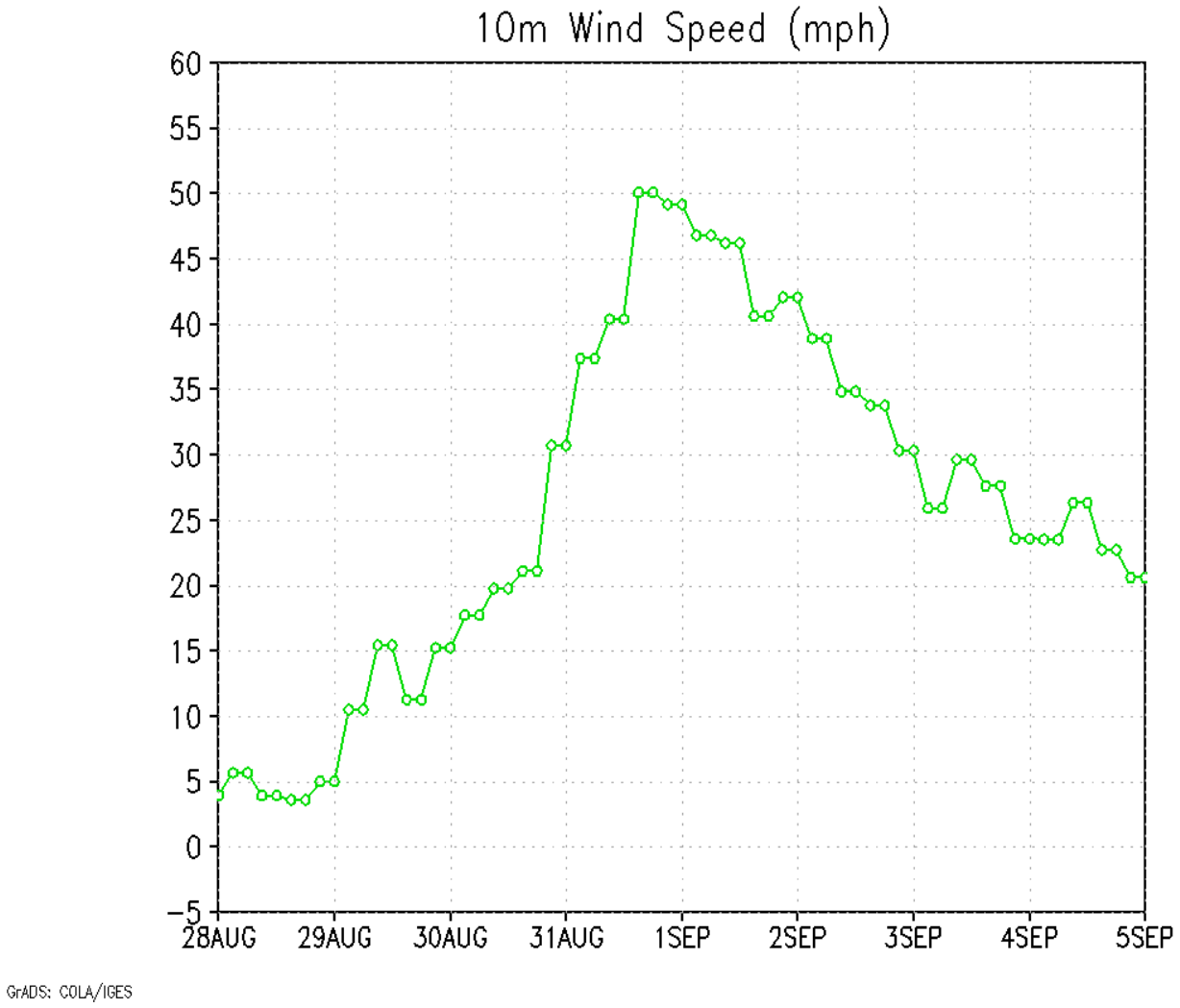

Figure 21. Simulated 10 meter wind speed in mph from August 28 to September 5.

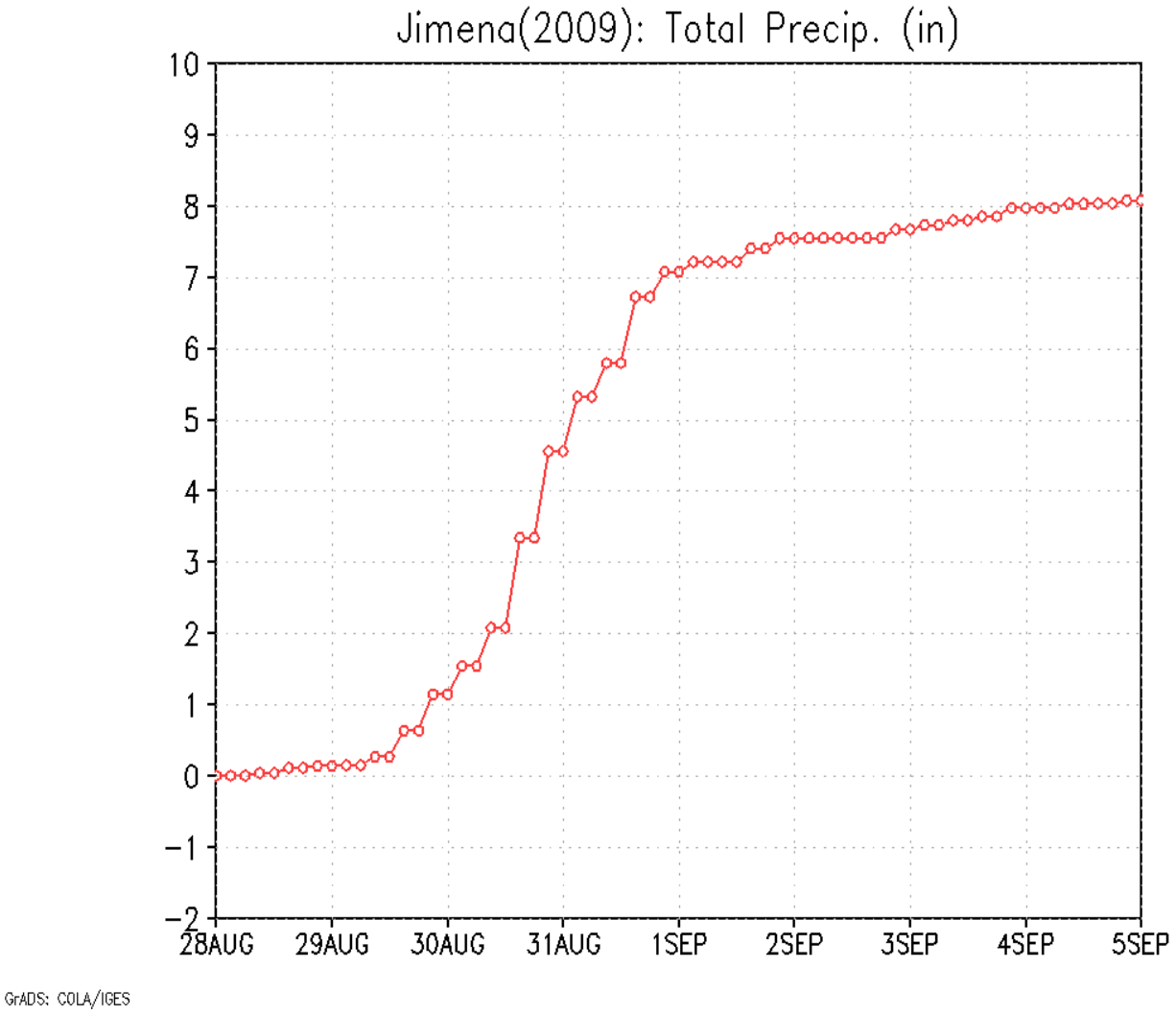

Figure 22. Total precipitations in inches from August 28 to September 5.

5.3 DA Experiment

The analysis obtained from WRFDA was used to initialize the WRF-ARW model and the rest of perimeters kept the same as the control experiment. This experiment was conducted to examine the capability of the DA approach to improve upon the storm track and intensity of the storm or forecast. The maximum wind speed, minimum sea level pressure and the storm track of the DA experiment are compared with the control experiment. The simulation with the data assimilation recorded the highest wind intensity compared to the control experiment (Figure 23).

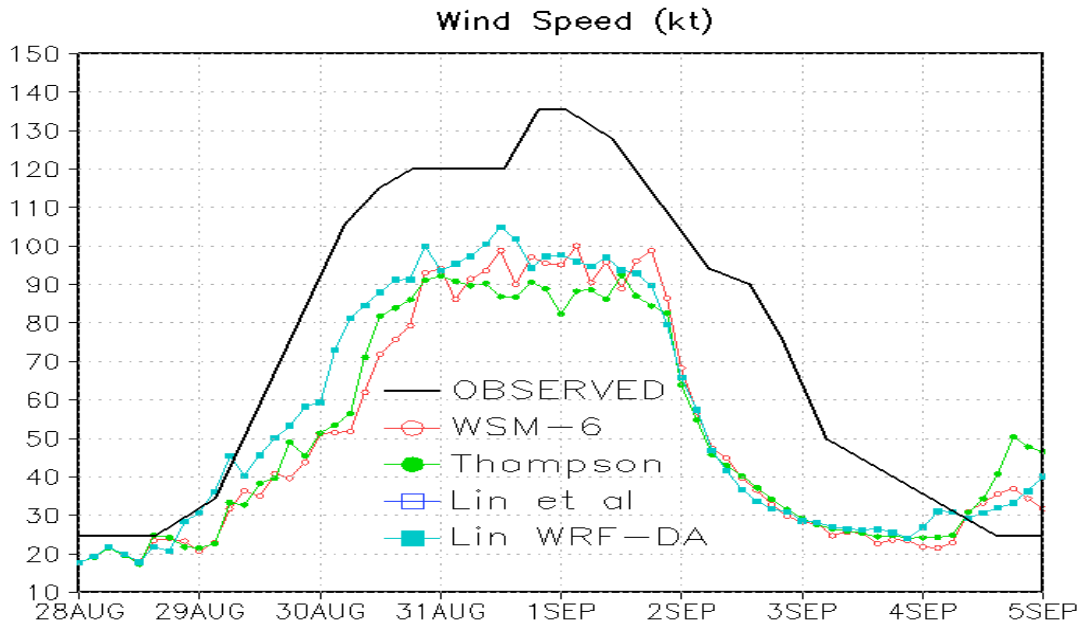

Figure 23. Comparison of wind intensity of Jimena 2009 observed from NHC with WRF simulation using WSM-6, Thompson, Lin et al and WRFDA.

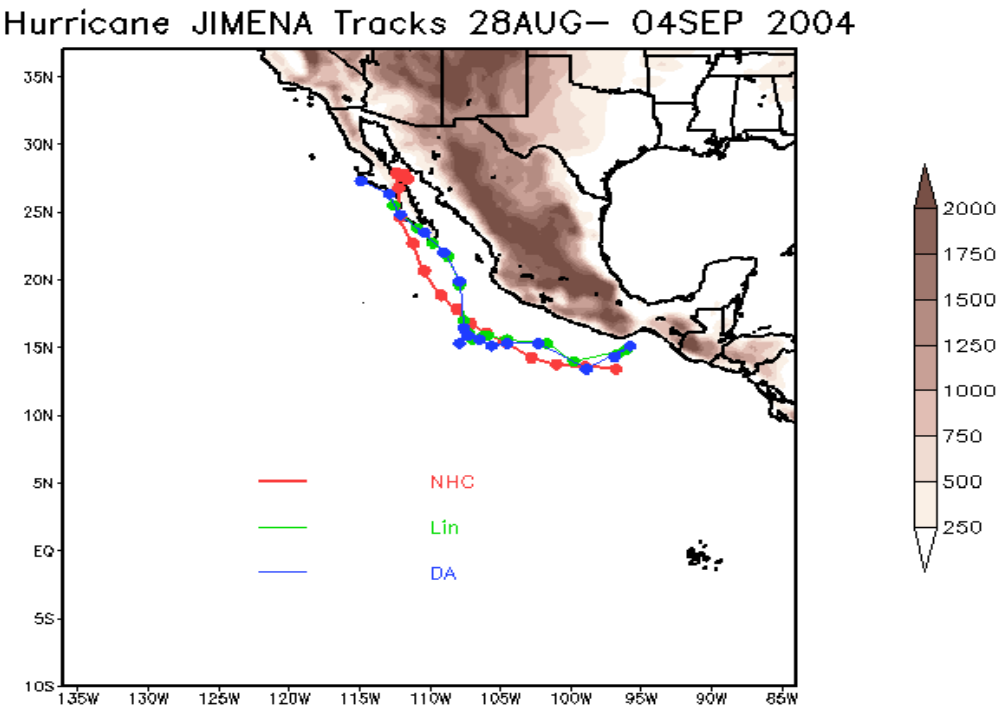

Figure 24. Comparison of TCs best tracks from NHC with simulation Control experiment and the WRFDA.

Figure 24 compares the observed track NHC with the control and experiment. Both tracks from the WRF simulations followed closely to the observed track. They have much smaller error at the beginning of simulation compared to the observed track. Both sway a few miles to the left of the observed track at location of landfall. There were no significant differences between the track with the data assimilation and the one without DA.

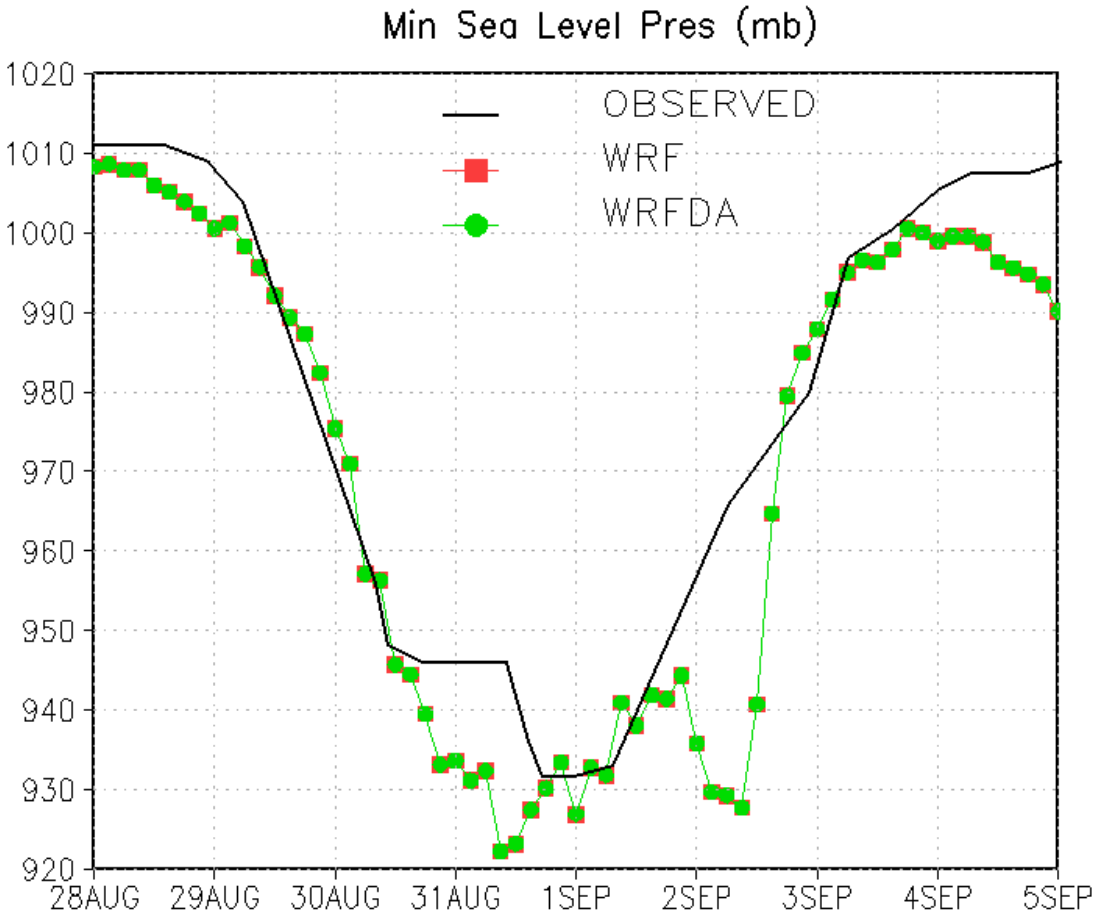

Figure 25. Minimum sea level pressures (mb) of the observation, control and the DA experiments. The result is based on the 30-km resolution.

CHAPTER 6

Conclusion and Future Research

6.1 Summary

This research studied the association of African Easterly Waves (AEW), mesoscale convective systems with tropical cyclones activities in the northeast Pacific Ocean. Using infrared satellite imagery and NCEP FNL (Final) Operational Global Analysis we were able to relate the cyclogenesis of Jimena to Africa easterly waves and its associated MCS. The study also analyzes the orographic influence of the Central America and Mexico America on development of tropical cyclones in this basin.

Six sensitivity tests were conducted in order to set up a suitable control experiment for this study. The first three sensitivity experiments examined the influence of initial conditions on WRF-ARW simulations of Hurricane Jimena (2009). We evaluated 700mb relative vorticity, u10 wind, surface temperature and sea level pressure under three different initial conditions. Significant differences were observed in term of the position of the storm. The result shows the tracks obtained from the two simulations on 25 August and 27 August at 00Z were approximately 24 hours ahead of that of the 28/Z00Z simulation and the observed track. The result shows the two simulations initialized on 25 00Z and 27 00Z were approximately 24 hours ahead of the 28/Z00Z and the observed. However no significant differences were observed in terms of sea level pressure surface temperature and relative vorticity. Thus the findings suggest WRF-ARW model is quite sensitive to the time when model is initialized. The three remaining sensitivity test were performed to choose the best microphysics scheme for the control experiment. The Lin et al, WSM6 and the Thompson schemes were implemented and compared with the best track and intensity from NHC. The Lin et al microphysics scheme performed

slightly better compared to the rest of the schemes with respect to maximum wind speed. Again the Lin et al scheme has a slight edge over the WSM-6 and Thompson schemes on storm track and minimum sea level pressure.

Finally this paper analyzes the impact of 3DVAR on storm track and intensity using WRFDA. The findings reveal optimal impact of 3DVAR and some improvement in u10m wind speed (m/s). The wind speed of the DA experiment was slightly higher than the control experiment (without DA). On the other hand, the DA did not have any significant impact on minimum sea level pressure and storm track.

6.2 Future Work

Future work includes performing 3DVAR with more observational data in order to find out whether there will be any improvement of the tropical cyclone intensity and track. Also I will vary other ARW-WRF physics options such as cumulus parameterization, short wave and longwave radiation schemes to examine whether model forecast will be improved.

References

Avila, L. A., and G. B. Clark, 1989: Atlantic tropical systems of 1988. *Mon. Wea. Rev.,* **117,** 2260–2265.

Avila, L. A., and R. J. Pasch, 1992: Atlantic tropical systems of 1991. *Mon. Wea. Rev.,* **120,** 2688–2696.

Barker, D. M., W. Huang, Y.-R. Guo, A. J. Bourgeois, Q. N. Xiao, 2004: A Three-Dimensional Variational Data Assimilation System for MM5: Implementation and Initial Results. *Mon. Wea. Rev.*, **132**, 897–914.

Barker, D. M., W. Huang, Y.R. Guo, and A. Bourgeois, 2003: A three-dimensional variational (3DVAR) data assimilation system for use with MM5. NCAR Tech. Note NCAR/TN-4531STR, 68 pp. [Available from UCAR Communications, P.O. Box 3000, Boulder, CO 80307.]

Beven, J. L., 2009: Hurricane Jimena (EP132009). National Hurricane Center Tropical Cyclone Report, *http://www.nhc.noaa.gov/pdf/TCR-EP132009_Jimena.pdf.*

Bowman, W. N., & , R. J. Renard, 1976: The Climatology and Forecasting of Eastern North Pacific Ocean Tropical Cyclones. *Naval Environmental Prediction Research Facility Tech. Paper*, **79**,7–76.

Burpee, R. W., 1972: The origin and structure of easterly waves in the lower troposphere of North Africa. *J. Atmos. Sci.*, **29,** 77–90.

Carlson, T. N., 1969: Some remarks on African disturbances and their progress over the tropical Atlantic. *Mon. Wea. Rev.*, **97**, 716– 726.

Charney JG et al (1950) Numerical integration of the barotropic vorticity equation. *Tellus*,**2**, 237–254

Charney JG et al (1969) Use of incomplete historical data to infer the present state of the atmosphere. *J. Atmos Sci.,* **2**,1160–1163.

Cucurull, L., F. Vandenberghe, D. Barker, E. Vilaclara & A. Rius, 2004: Three-dimensional variational data assimilation of ground-based GPS ZTD and meteorological observations during the 14 December 2001 storm event over the western Mediterranean Sea. *Monthly weather review*, *132*(3), 749-763.

Deng, A., Stauffer, D. R., Zielonka, J. R., & Hunter, G. K., 2007: A comparison of high-resolution mesoscale forecasts using MM5 and WRF-ARW for the 2006 Winter Olympics. Proceedings of the 8th WRF/ MM5 Users' Workshop, NCAR, Boulder, Colorado.

Fan, X., Tilley, J. S., & Walsh, J. E., 2004: Application of MM5/3DVAR at High Latitude: Resolution Sensitivity. In *Preprints, 5 th WRF/14 th MM5 Users' Workshop* (pp. 22-25).

Farfan, L. M., and J. A. Zehnder, 1997: Orographic influence on the synoptic-scale circulations associated with the genesis of Hurricane Guillermo (1991). *Mon. Wea. Rev.,* **125,** 2683–2698.

Frank, W. M., and, P. E Roundy, 2006: The role of tropical waves in tropical cyclogenesis. *Monthly weather review*, *134*(9), 2397-2417.

Gray, W. M., 1968: Global view of the origin of tropical disturbances and storms. *Mon. Wea. Rev*., **96**, 669-700

Hurricane Season 2009: Hurricane Jimena (Eastern Pacific), http://www.nasa.gov/mission_pages/hurricanes/archives/2009/h2009_Jimena.html

Kalnay E (2003) Atmospheric modeling, data assimilation and predictability. Cambridge University Press, Cambridge, p 341

Kimberlain, T. B., and Brennan, M. J.,2011: Eastern North Pacific Hurricane Season of 2009. *Monthly Weather Review*, *139*(6), 1657-1672.

Lin, Y. L., Mesoscale Dynamics. Cambridge: Cambridge University Press, 2007.

Mexico, http://www.worldatlas.com/webimage/countrys/namerica/mx.htm

Molinari, J., and D. Vollaro,2000: Planetary- and Synoptic-Scale Influences on Eastern Pacific Tropical Cyclogenesis: *Mon. Wea. Rev*., **128**,3296-3307.

Molinari, J., D. Vollaro, S. Skubis, and M. Dickinson, 2000: Origins and mechanisms of eastern Pacific tropical cyclogenesis: a case study. *Mon. Wea. Rev*., **128**, 125-139.

NCEP FNL Operational Model Global Tropospheric Analyses, *http://dss.ucar.edu/datasets*

Navon, I. M. (2009). Data assimilation for numerical weather prediction: a review. *Data Assimilation for Atmospheric, Oceanic, and Hydrologic Applications*, *18*(475), 326.

Rawlins, F., Ballard, S. P., Bovis, K. J., Clayton, A. M., Li, D., Inverarity, G. W., ... & Payne, T. J.,2007: The Met Office global four-dimensional variational data assimilation scheme. *Quarterly Journal of the Royal Meteorological Society*, **133**, 347-362.

Raymond, D. D., López-Carrillo, C., & Cavazos, L. L. (2006). Case-studies of developing east Pacific easterly waves. *Quarterly Journal of the Royal Meteorological Society*, *124*(550), 2005-2034.

Richardson LF (1922) Weather prediction by numerical processes. Cambridge University Press. Reprinted by Dover (1965, New York).

Robertson, K.E., 2004: The maintenance and propagation of African easterly waves across northern Africa: A case study and analysis of the environment.

Skamarock, W. C., Klemp, J. B., Dudhia, J., Gill, D. O., Barker, D. M., Wang, W., & Powers, J. G. (2005). *A description of the Advanced Research WRF Version 2* (No. NCAR/TN-468+

STR). National Center for Atmospheric Research Mesoscale and Microscale Meteorology Division, Boulder, CO.

University of Wisconsin-Madison, Space Science and Engineering Center Geostationary Satellite Image Inventory, *http://www.ssec.wisc.edu/datacenter/*

Wang, B., Zou, X., & Zhu, J. (2000). Data assimilation and its applications. *Proceedings of the National Academy of Sciences, 97*(21), 11143-11144.

Whitney, L. D.,1995: The Relationship Between Sea Surface Temperature and Maximum Intensity of Tropical Cyclones in the Eastern North Pacific Ocean (No. AFIT/CI-95-106). AIR FORCE INST OF TECH WRIGHT-PATTERSON AFB OH.

WRF Model, http://www.mmm.ucar.edu/wrf/users/.

Zehnder, Joseph A., Donna M. Powell, David L. Ropp, 1999: The Interaction of Easterly Waves, Orography, and the Intertropical Convergence Zone in the Genesis of Eastern Pacific Tropical Cyclones. *Mon. Wea. Rev.*, **127**, 1566–1585.

Zehnder, Joseph A, and R. L. Gall, 1991a: On a mechanism for orographic triggering of tropical cyclones in the eastern North Pacific. *Tellus*, **43A,** 25–36.

Appendix A

Table 4

The min SLP (mb) result obtained from the NHC and sensitivity experimental (using 3 different MP), the mean and mean errors for SLP starting from 8/28/00Z to 9/04/00Z.

Forecast Period (h)	MSLP				ERROR			
		Result			Difference			
	NHC	Lin	WSM	Thmp	Lin	WSM	Thmp	OFCL
8/28/00Z	1008	1006	1007	1007	2	1	1	
8/28/12Z	1008	1006	1005	1006	2	3	2	
8/29/00Z	1005	1001	1002	1003	4	3	2	
8/29/12Z	990	992	995	998	2	5	8	
8/30/00Z	970	975	983	986	5	13	16	
8/30/12Z	948	946	954	959	2	6	11	
8/31/00Z	945	934	938	943	15	7	2	
8/31/12Z	945	923	935	944	22	10	1	
9/01/00Z	931	927	939	950	4	8	19	
9/01/12Z	940	938	937	949	2	3	9	
9/02/00Z	957	936	926	938	21	31	19	
9/02/12Z	971	934	920	916	37	51	55	
9/03/00Z	985	917	927	913	68	58	72	
9/03/12Z	999	914	935	965	85	64	34	
9/04/00Z	1004	928	950	992	76	54	12	
AVE	974	952	957	965	23	21	18	

Table 5

The observed, sensitivity experiment u10m wind speed (m/s) and experimental error starting from 08/28/00Z to 09/04/00Z.

	Speed/Error (kt)												
	NHC	25th		26th		28th		LIN		WSM6		Thmp	
		Sp	Er	Sp	Er	Sp	Er	Sp	Er	Sp	Er	Sp	Er
8/28/00Z	25							20	5	21	4	20	5
8/28/12Z	25							26	-1	27	-2	26	-1
8/29/00Z	35							30	5	30	5	27	8
8/29/12Z	60							49	11	40	20	38	22
8/30/00Z	90							69	21	55	35	51	39
8/30/12Z	115							89	26	90	25	82	33
8/31/00Z	120							97	23	94	26	92	28
8/31/12Z	120							101	19	94	26	87	33
9/01/00Z	135							100	35	97	38	82	53
9/01/12Z	125							99	26	95	30	92	33
9/02/00Z	105							86	19	92	13	90	15
9/02/12Z	90							96	-6	102	-12	91	-1
9/03/00Z	65							102	-37	95	-30	101	-36
9/03/12Z	45							95	-50	87	-42	83	-38
9/04/00Z	35							87	-52	74	-39	62	-27
Ave									22.4		23.1		24.8

Table 6

Observed and stimulated storm (Lin et al, wsm6, Thompson MP schemes) position starting from 08/28/00Z to 09/04/00Z.

Time	Best Track		Result					
	NHC		Lin		WSM6		Thompson	
	Lat (^oN)	Lon (^oW)	Lat (^oN)	Lon (^oW)	Lat (^oN)	Lon (^oW)	Lat (^oN)	Lon (^oW)
8/28/00Z	13.40	96.80	14.50	96.70	14.50	96.70	14.5	96.7
8/28/12Z	13.50	99.00	14.80	96.10	12.60	99.50	14.8	96.1
8/29/00Z	13.70	101.00	14.00	99.80	13.70	99.20	13.4	99.2
8/29/12Z	14.20	102.90	15.30	101.70	15.10	101.40	14.8	101.2
8/30/00Z	15.40	104.70	15.60	104.50	14.80	103.90	14.8	104.5
8/30/12Z	16.00	106.00	15.90	105.90	15.30	105.30	15.1	105.9
8/31/00Z	16.70	107.10	15.90	106.20	15.90	106.70	15.3	107.3
8/31/12Z	17.70	108.20	15.60	107.00	15.90	106.50	14.8	107.6
9/01/00Z	18.90	109.40	16.10	107.30	15.90	106.70	15.1	107.9
9/01/12Z	20.60	110.50	17.00	107.60	17.00	106.70	16.2	107.9
9/02/00Z	22.40	111.40	19.60	107.90	19.30	107.90	19.4	108.1
9/02/12Z	24.60	112.00	21.70	108.70	21.20	109.00	21.2	110.1
9/03/00Z	26.70	112.40	22.70	109.80	24.30	110.70	22.2	111.8
9/03/12Z	27.60	112.30	23.80	110.90	25.00	112.30	24.3	112.9
9/04/00Z	27.60	111.90	25.50	112.60	26.30	113.50	26.3	112.9

Table 7

Distance between the observed storm track and each of stimulated storm tracks from 08/28/00Z to 09/04/00Z.

Time	Distance(km)					
	25th	26th	28th	Lin	WSM6	Thmp
8/28/00Z				122.8	122.8	122.8
8/28/12Z				344.5	113.8	344.5
8/29/00Z				133.8	194.5	197.4
8/29/12Z				177.8	189.9	194.8
8/30/00Z				30.9	108.8	70.1
8/30/12Z				15.4	108.1	100.6
8/31/00Z				130.9	98.7	157.1
8/31/12Z				266.2	269.8	328.8
9/01/00Z				382.8	439.7	451.6
9/01/12Z				503.4	565.8	560.9
9/02/00Z				478.4	501.0	478.3
9/02/12Z				466.7	487.1	425.2
9/03/00Z				516.5	316.7	504.0
9/03/12Z				445.2	289.1	371.8
9/04/00Z				243.7	214.6	175.3
Ave				283.9	268.0	298.9

Table 8

Observed and stimulated storm (control experiment and 3DVAR simulation) position starting from 08/28/00Z to 09/04/00Z.

Time	Best Track		Result			
	NHC		CNTR		DA	
	Lat (^oN)	Lon (^oW)	Lat (^oN)	Lon (^oW)	Lat (^oN)	Lon (^oW)
8/28/00Z	13.40	96.80	14.50	96.7.0	14.30	96.90
8/28/12Z	13.50	99.00	14.80	96.10	15.10	95.80
8/29/00Z	13.70	101.00	14.00	99.80	13.40	98.90
8/29/12Z	14.20	102.90	15.30	101.70	15.30	102.30
8/30/00Z	15.40	104.70	15.60	104.50	15.30	104.50
8/30/12Z	16.00	106.00	15.90	105.90	15.10	105.60
8/31/00Z	16.70	107.10	15.90	106.20	15.60	107.30
8/31/12Z	17.70	108.20	15.60	107.00	15.90	106.50
9/01/00Z	18.90	109.40	16.10	107.30	15.30	107.90
9/01/12Z	20.60	110.50	17.00	107.60	16.40	107.60
9/02/00Z	22.40	111.40	19.60	107.90	19.90	107.90
9/02/12Z	24.60	112.00	21.70	108.70	22.00	109.00
9/03/00Z	26.70	112.40	22.70	109.80	23.50	110.40
9/03/12Z	27.60	112.30	23.80	110.90	24.80	112.10
9/04/00Z	27.60	111.90	25.50	112.60	26.30	112.90

Table 9

Distance between the simulated storm track and observed best track, maximum u10m wind speed and the experimental error starting from 08/28/00Z to 09/04/00Z.

Time	Track		Max Wind Speed (ms^{-1})				
	Distance		Speed			Error	
	CNTR	DA	NHC	CNTR	DA	CNTR	DA
8/28/00Z	122.8		25	20		5	
8/28/12Z	344.5		25	26		1	
8/29/00Z	133.8		35	30		5	
8/29/12Z	177.8		60	49		11	
8/30/00Z	30.9		90	69		21	
8/30/12Z	15.4		115	89		26	
8/31/00Z	130.9		120	97		23	
8/31/12Z	266.2		120	101		19	
9/01/00Z	382.8		135	100		35	
9/01/12Z	503.4		125	99		26	
9/02/00Z	478.4		105	86		19	
9/02/12Z	466.7		90	96		6	
9/03/00Z	516.5		65	102		37	
9/03/12Z	445.2		45	95		50	
9/04/00Z	243.7		35	87		52	
Ave	284		79	76		22	

Table 10

NHC official (OFCL), climatology-persistence skill baseline (OCD5) and WRF simulation track forecast errors (n mi) for Hurricane Jimena, 28 August – 4 September 2009. Errors that are smaller than the five-year means are shown in boldface type.

Model	Forecast Period (h)						
	12	24	36	48	72	96	120
OFCL (Jimena)	**23.3**	**43.5**	**58.9**	**64.4**	**52.4**	**109.4**	218.8
OCD5 (Jimena)	34.0	71.5	116.8	157.0	241.0	372.2	503.4
Forecasts	26	24	22	20	16	12	8
CNTR	31.0	51.7	71.7	90.2	123.6	161.3	201.8
DA	38.4	73.6	111.9	149.1	214.2	261.1	311.5

Table 11

NHC official (OFCL) and climatology-persistence skill baseline (OCD5) WRF simulation and intensity forecast errors (kt) for Hurricane Jimena, 28 August – 4 September 2009.

Model	Forecast Period (h)						
	12	24	36	48	72	96	120
OFCL (Jimena)	6.9	10.4	14.1	11.5	12.5	10.0	8.9
OCD5 (Jimena)	8.6	13.1	15.8	17.2	25.6	26.0	22.12
Forecasts	26	24	22	20	16	12	8
CNTR							
DA							

Appendix B

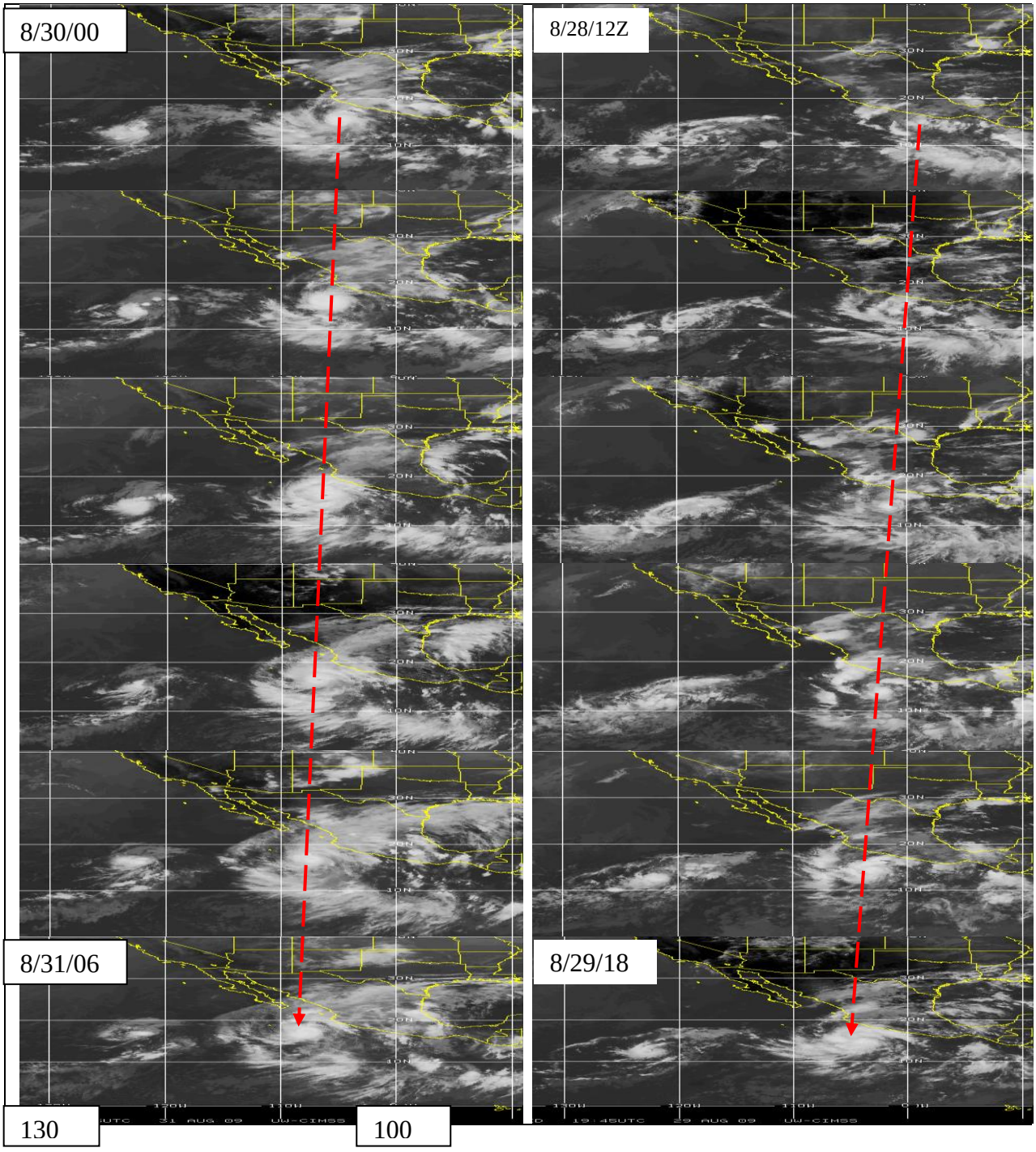

Figure 26. GOES-WEST infrared satellite imagery showing cloud top temperature of Hurricane Jimena from 12Z 28 August to 06Z 31 August on 6-hr intervals provided by UW-CIMSS.

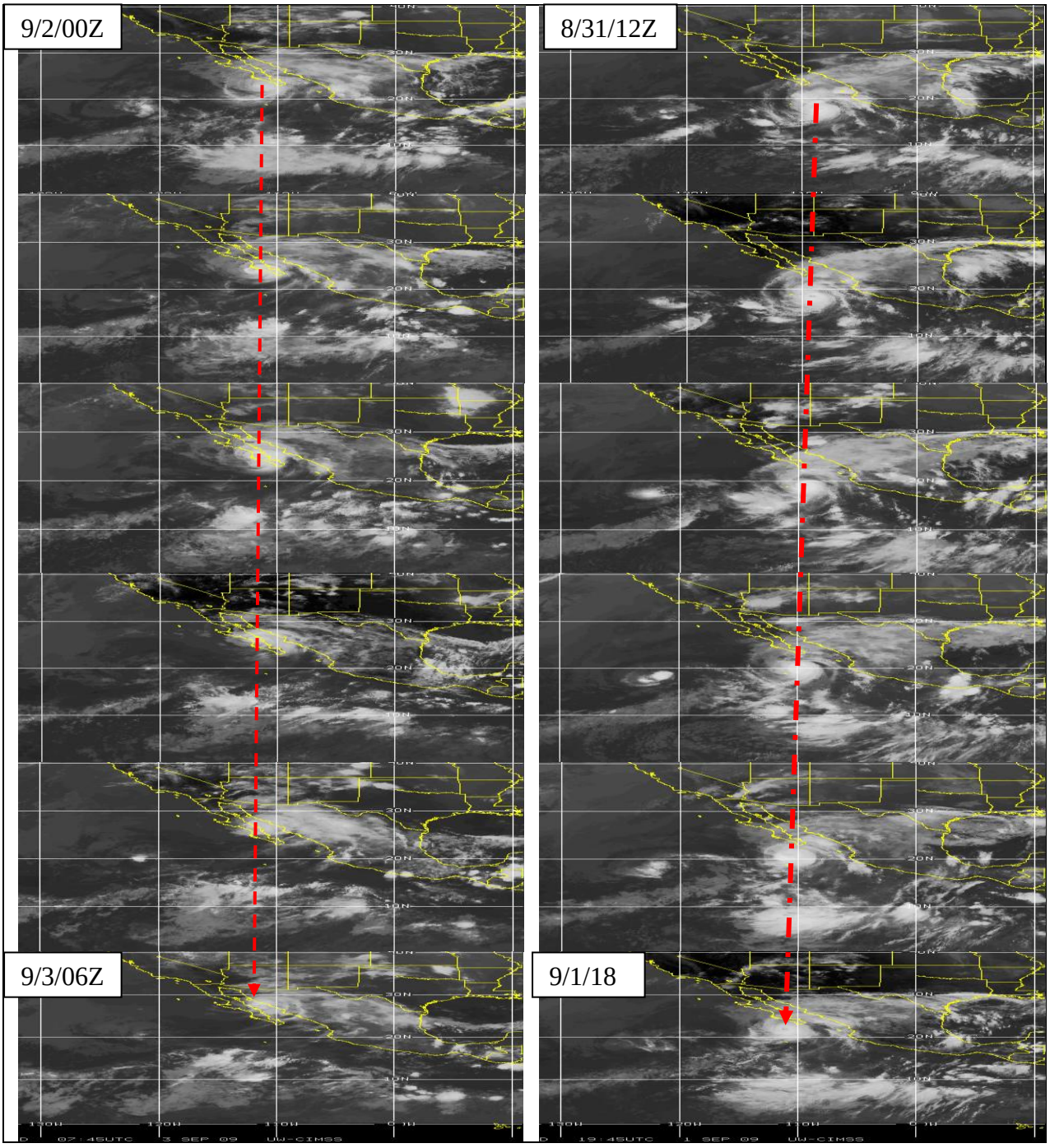

Figure 27. GOES-WEST infrared satellite imagery showing cloud top temperature of Hurricane Jimena from 12Z 31 August to 06Z 3 Sept. on 6-hr intervals provided by UW-CIMSS.

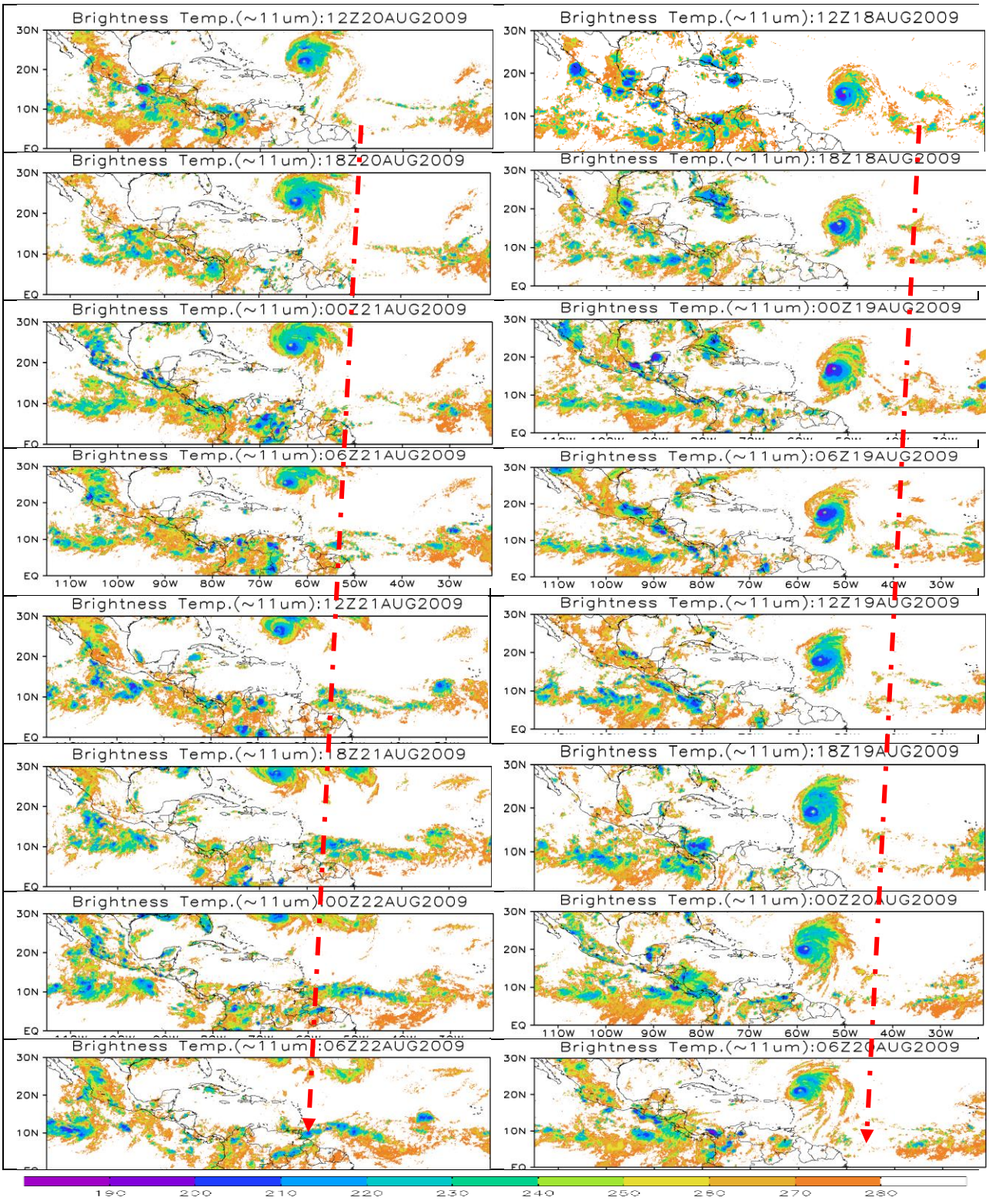

Figure 28. Brightness Temperature derived from the Gridded Satellite data for 8/18/12Z to 8/22/06Z.

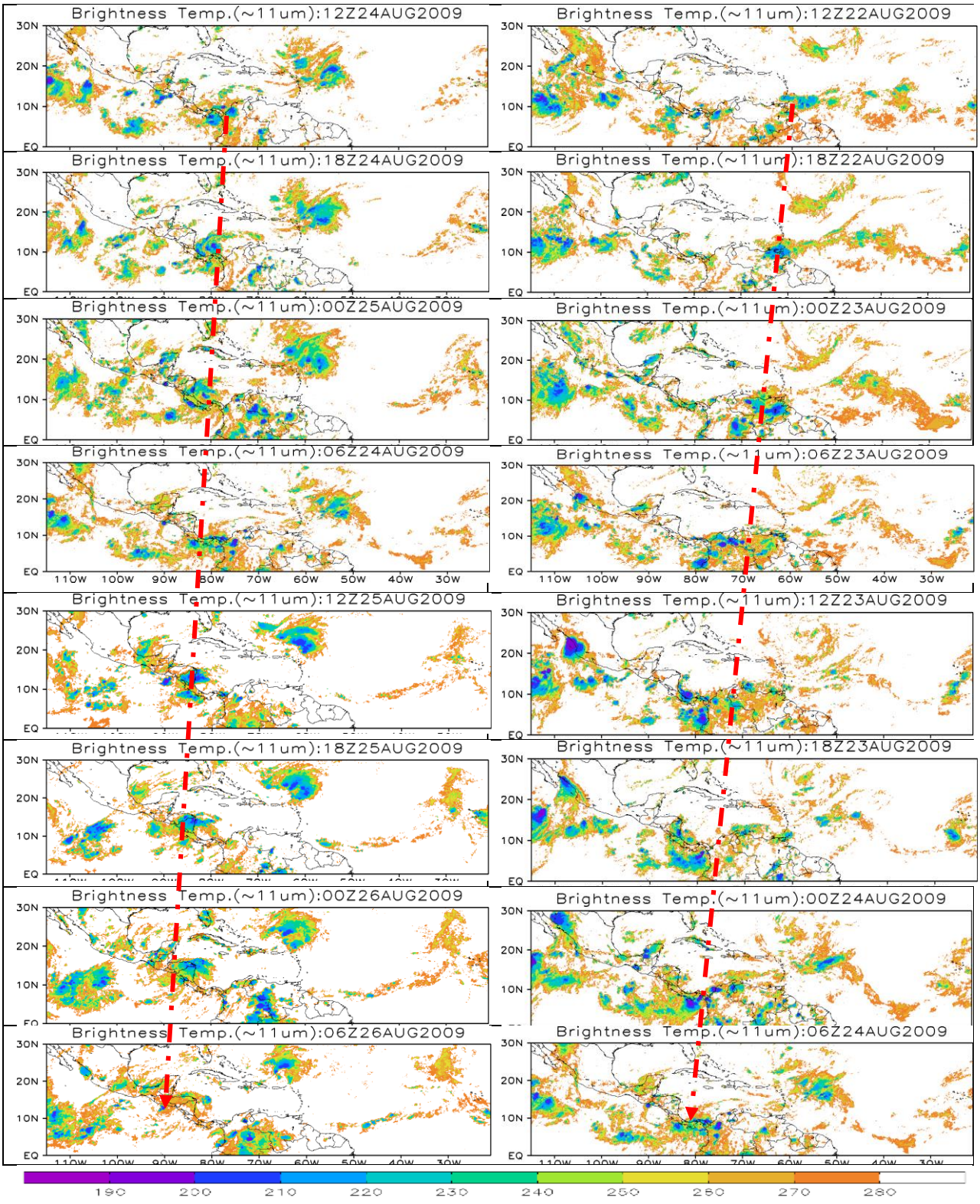

Figure 29. Brightness Temperature derived from the Gridded Satellite data for 8/22/12Z to 8/26/06Z.

Appendix C

Displayed in the below plots are relative vorticity obtained from the gridded atmospheric motion vector output u and v atmospheric motion vector components at the 500 mb by the University of Wisconsin-Madison Cooperative Institute for Meteorological Satellite Studies (UW-CIMSS). UW-CIMSS computed these vorticity using finite differencing of (dv/dx - du/dy), where *u* and *v* are the wind components and x and y are the horizontal grid spacing. Relative vorticity denoted by Color contour.

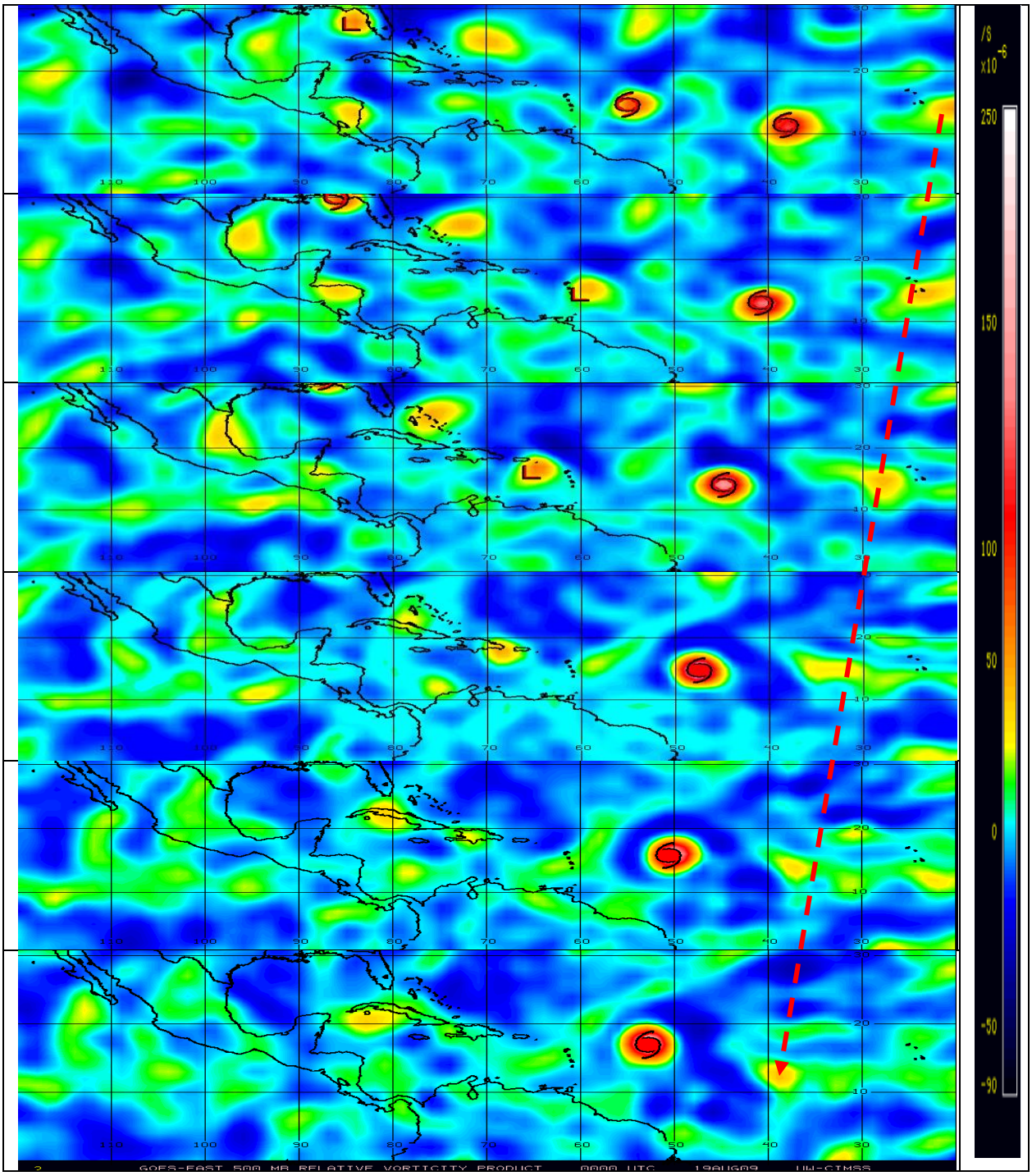

Figure 30. GOES-EAST 500-mb Relative Vorticity (overlay) between 8/16/12Z and 8/19/00Z for every 12hrs intervals derived from atmospheric motion vector output *u* and *v* components by UW-CIMSS

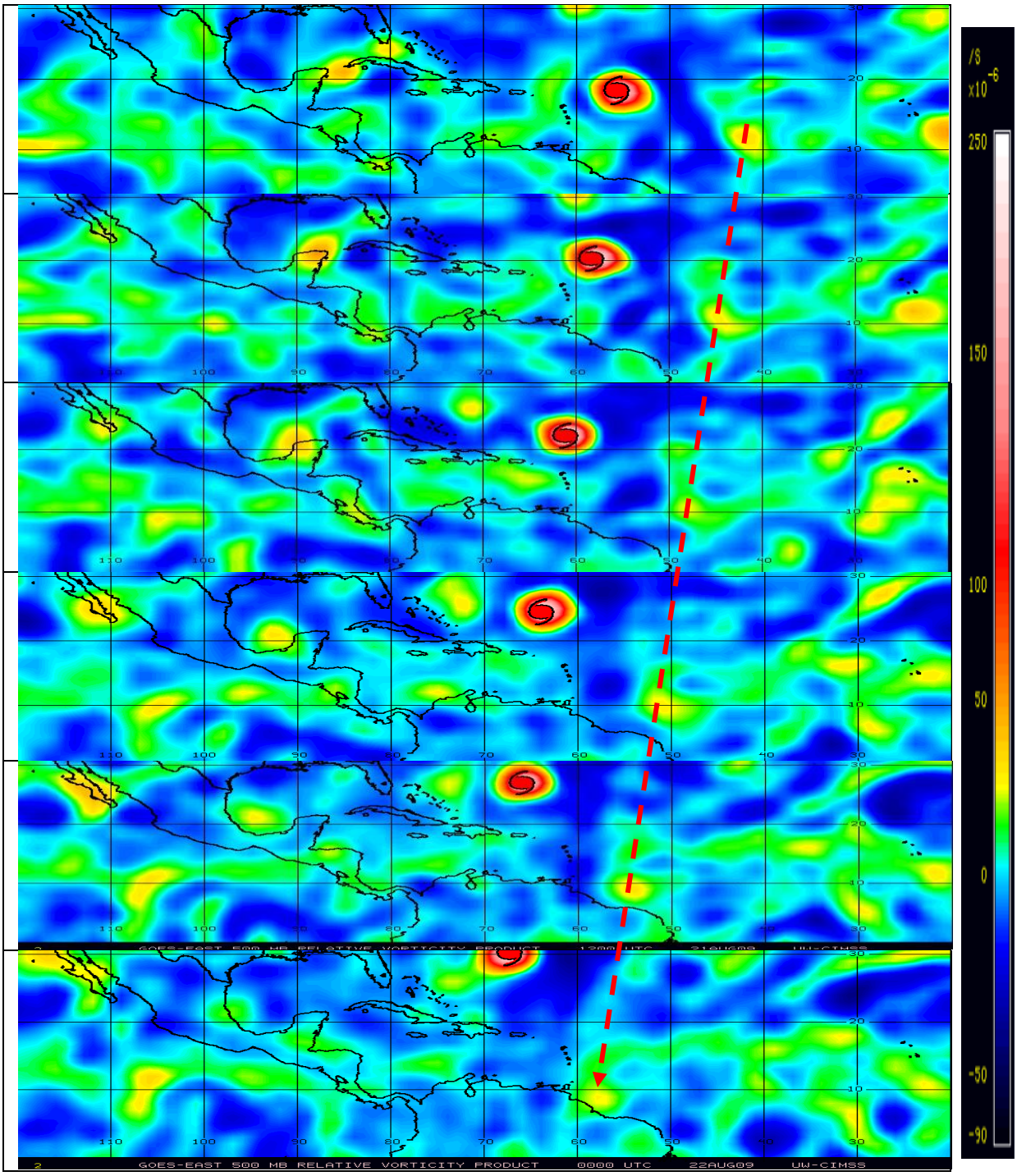

Figure 31. GOES-EAST 500-mb Relative Vorticity (overlay) between 8/19/12Z and 8/22/00Z for every 12hrs intervals derived from atmospheric motion vector output u and v components by UW-CIMSS.

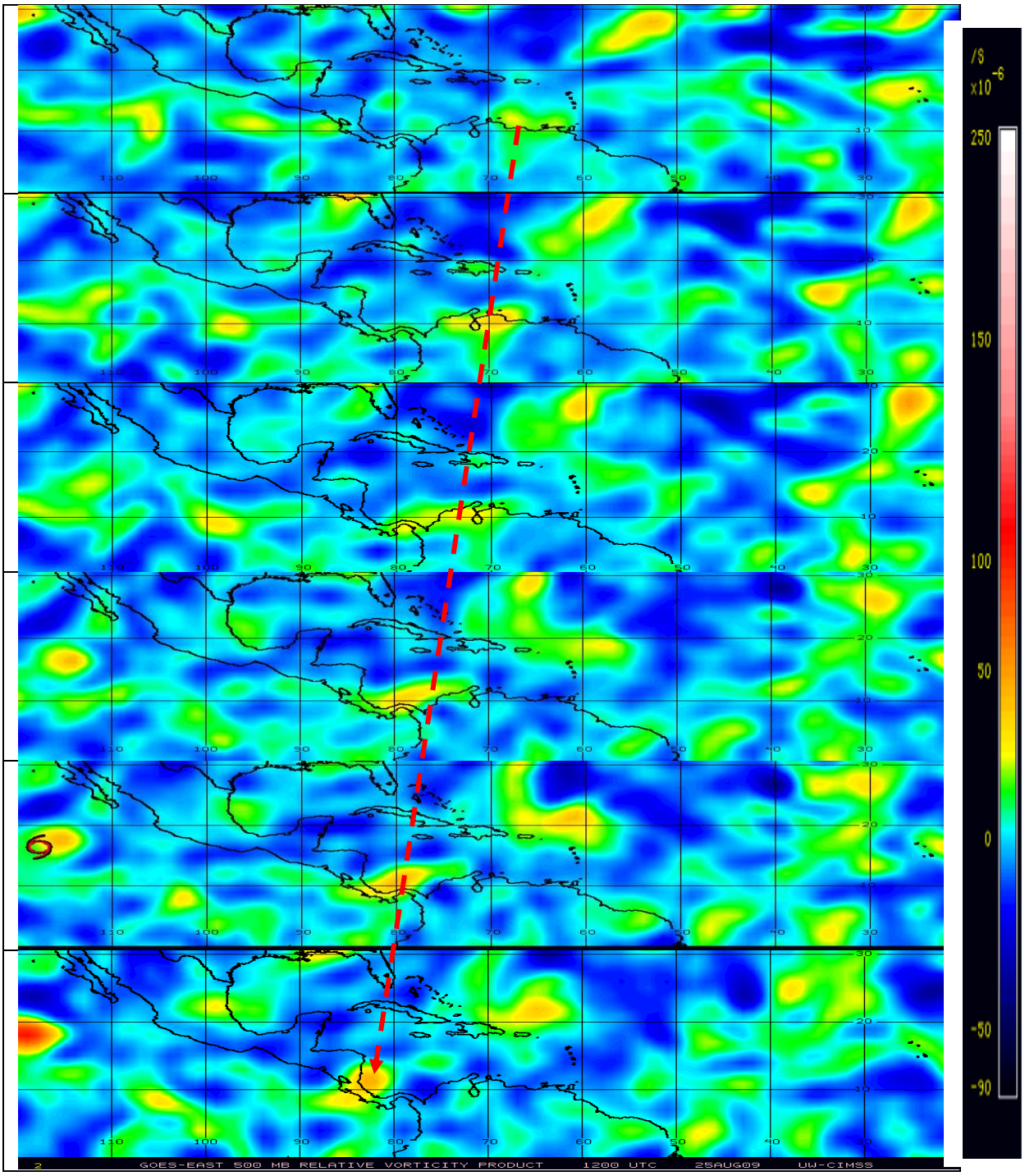

Figure 32. GOES-EAST 500-mb Relative Vorticity (Overlay) between 8/22/12Z and 8/25/12Z for every 12hrs intervals derived from atmospheric motion vector output u and v components by UW-CIMSS.

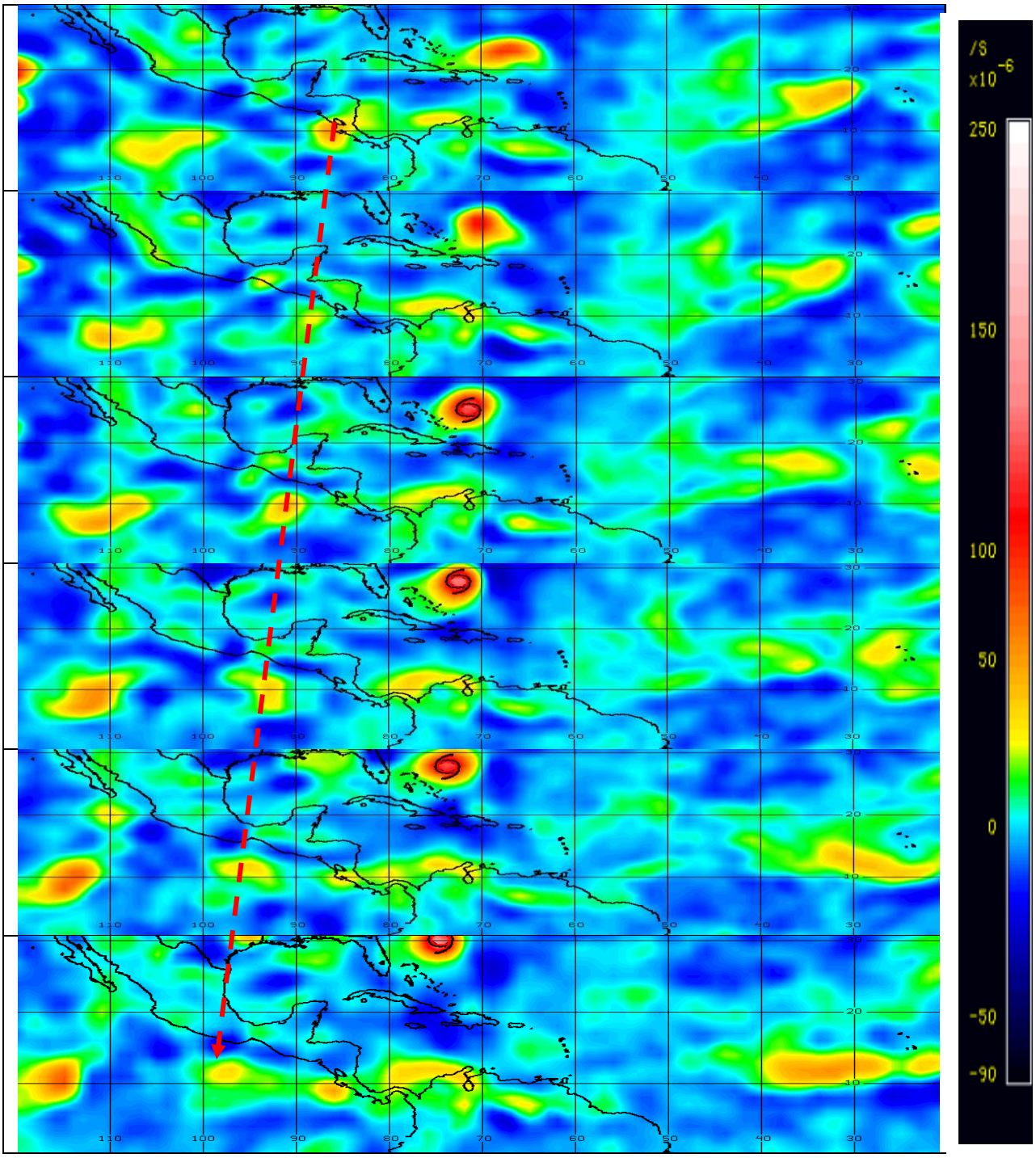

Figure 33. GOES-EAST 500-mb Relative Vorticity (overlay) between 8/26/00Z and 8/28/00Z for every 12hrs intervals derived from atmospheric motion vector output u and v components by UW-CIMSS.

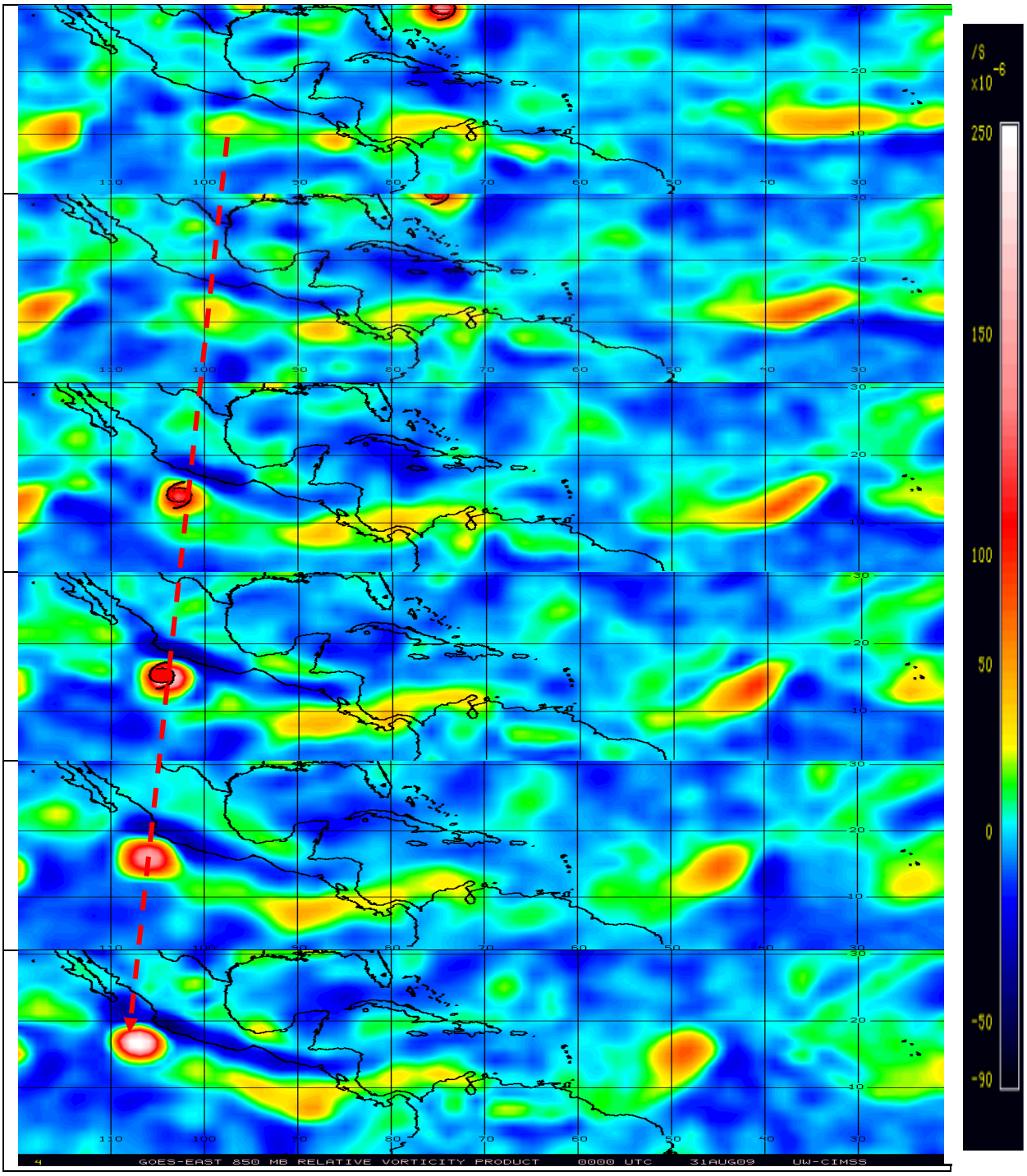

Figure 34. GOES-EAST 500-mb Relative Vorticity (overlay) between 8/28/12Z and 8/31/00Z for every 12hrs intervals derived from atmospheric motion vector output u and v components by UW-CIMSS.

Appendix D

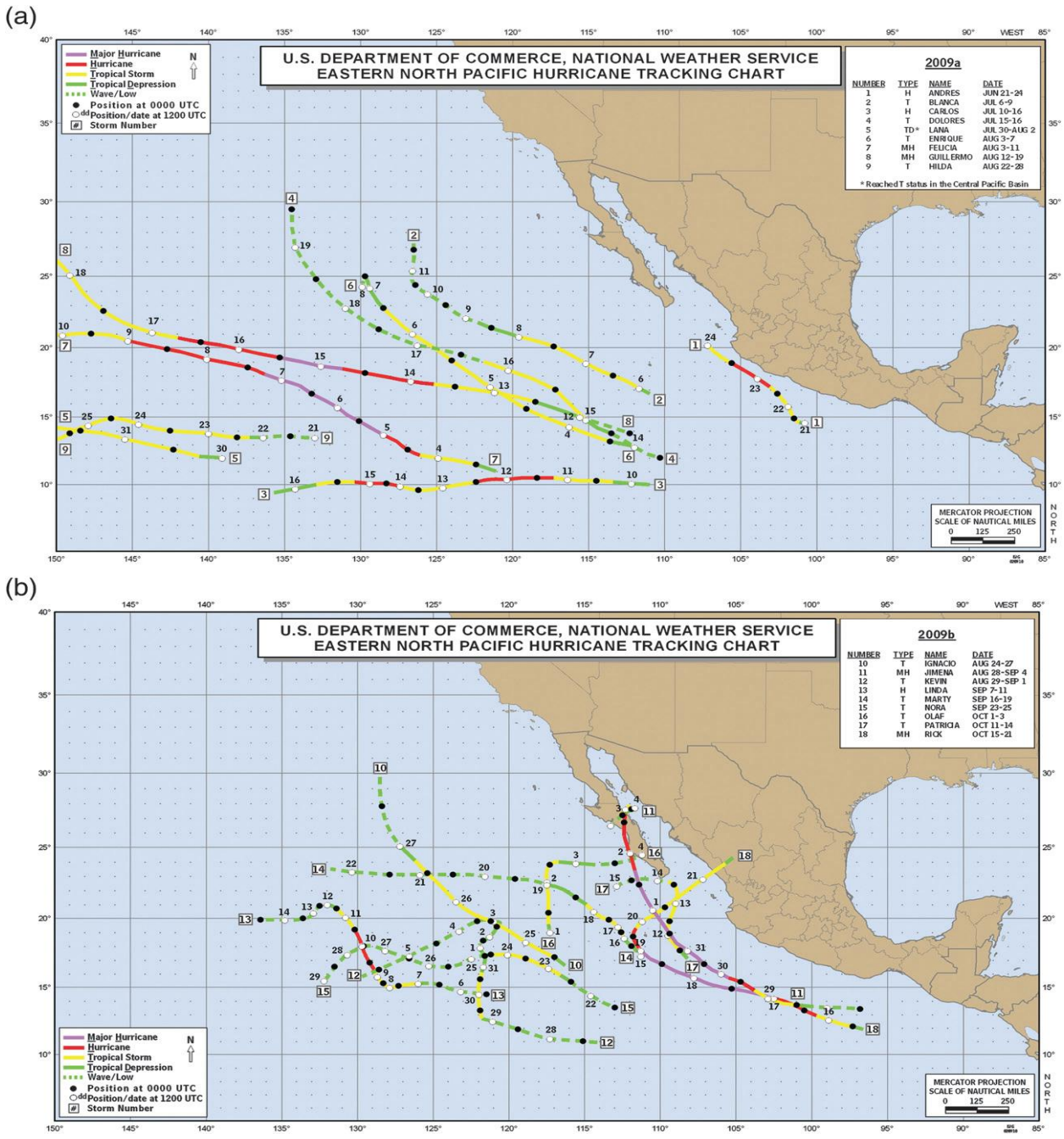

Figure 35. (a) Tracks of the first eight tropical storms and hurricanes in the eastern North Pacific basin in 2009 (including remnant low stage) and Tropical Storm Lana, which was named in the central North Pacific basin. (b) Tracks of the final nine tropical storms and hurricanes in the eastern North Pacific basin in 2009, including remnant low stage.

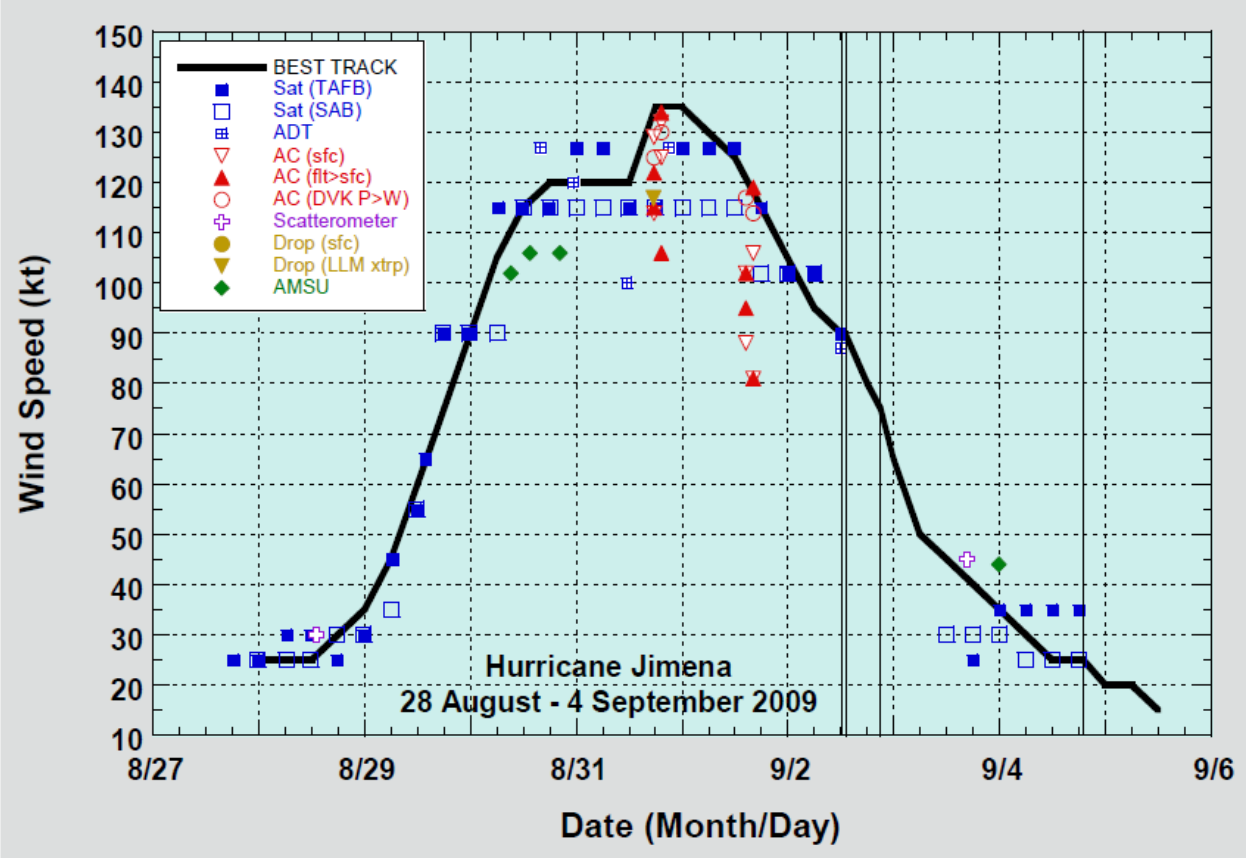

Figure 36. Selected wind observations and best track maximum sustained surface wind speed curve for Hurricane Jimena, 28 August – 4 September 2009. Dashed vertical lines correspond to 0000 UTC. Solid vertical lines denote landfalls.

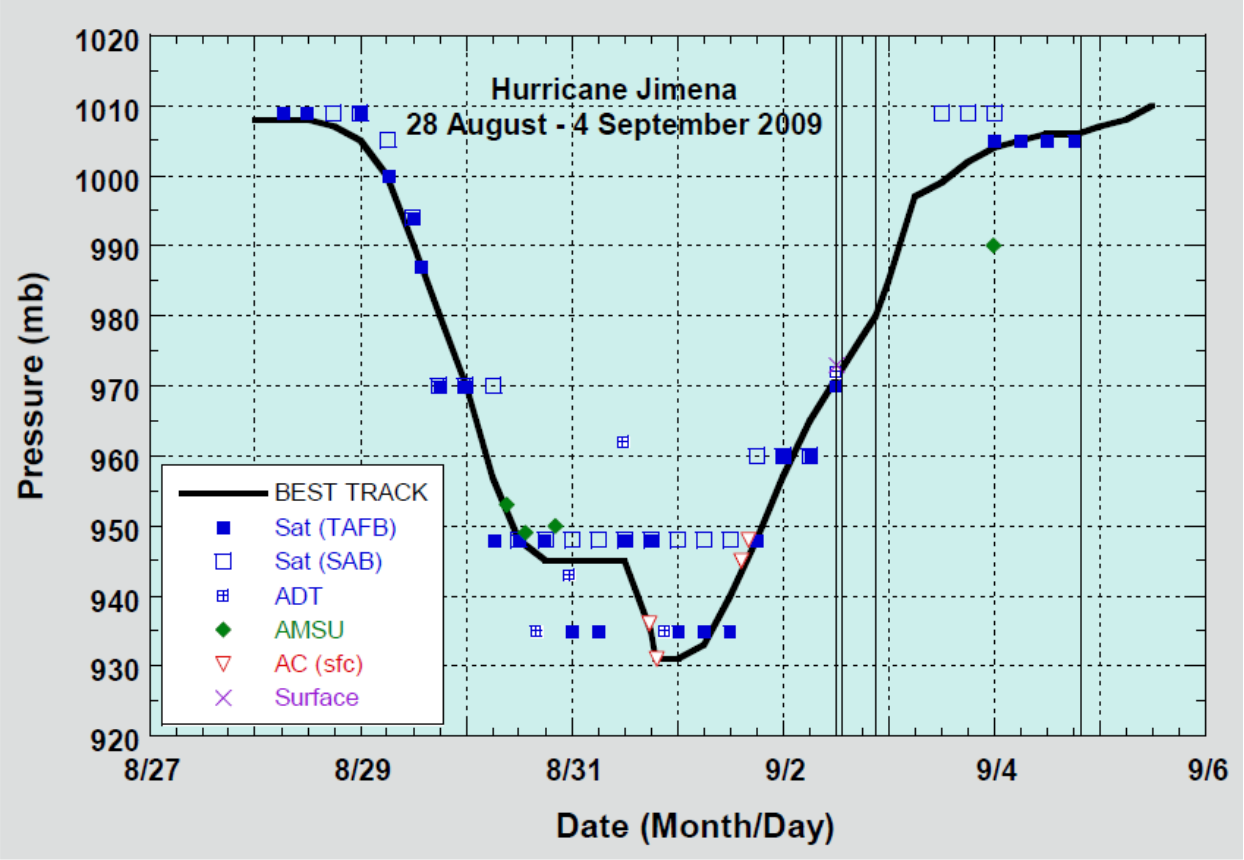

Figure 37. Selected pressure observations and best track minimum central pressure curve for Hurricane Jimena, 28 August – 4 September 2009. Dashed vertical lines correspond to 0000 UTC. Solid vertical lines denote landfalls.

Table 12

Selected surface observations for Hurricane Jimena, 28 August – 4 September 2009

Location	Minimum Level Pressure		Maximum Surface Wind Speed			Total Rain (in)
	Date/ Time (UTC)	Press. (mb)	Date/ Time (UTC)	Sustained (kt)	Gust (kt)	
MMGM – Guaymas, Sonora (27.9N 110.9W)			03/1442	25	50	26.46
Ciudad Constitution (Baja Cal.del Sur)	02/1350	976.5	02/1340	61	79	13.12
San Juanico (Baja Cal.del Sur)	02/2030	988.1	02/2110	38	63	
San Lucus (Baja Cal.del Sur)			01/2350	49	60	
Ciudad Obregon (Sonora) Cocoraque (Sonora)						3.01 3.96
El Cajoncito (Baja Cal.del Sur)						3.70
Empalme (Sonora) La Palmillita (Baja Cal.del Sur)						13.72 5.51
Loreto (Baja Cal.del Sur) Navojoa						4.08 4.65
San Bartolo (Baja Cal.del Sur)						5.39
Santa Rosalia (Baja Cal. del Sur)						6.59

Appendix E

WRF-ARW NAMELIST-INPUT

```
&time_control
 run_days                            = 8,
 run_hours                           = 00,
 run_minutes                         = 0,
 run_seconds                         = 0,
 start_year                          = 2009,   2009,   2009,
 start_month                         = 08,     08,     08,
 start_day                           = 28,     25,     25,
 start_hour                          = 00,     00,     00,
 start_minute                        = 00,     00,     00,
 start_second                        = 00,     00,     00,
 end_year                            = 2009,   2009,   2009,
 end_month                           = 09,     09,     09,
 end_day                             = 05,     02,     05,
 end_hour                            = 00,     00,     00,
 end_minute                          = 00,     00,     00,
 end_second                          = 00,     00,     00,
 interval_seconds                    = 21600,
 input_from_file                     = .true.,  .false.,  .false.,
 fine_input_stream                   = 0,      2,
 history_interval                    = 180,    180,    180,
 frames_per_outfile                  = 1,      1,      1,
 restart                             = .false.,
 restart_interval                    = 1440,
 io_form_history                     = 2,
 io_form_restart                     = 2,
 io_form_input                       = 2,
 io_form_boundary                    = 2,
 io_form_auxinput2                   = 2,
 auxinput1_inname                    = "met_em.d<domain>.<date>"
 auxinput4_inname                    = "wrflowinp_d01",
 auxinput4_interval                  = 360,
 io_form_auxinput4                   = 2,
 auxinput4_end_h                     = 0,
 debug_level                         = 0,

&domains
 time_step                           = 90,
 time_step_fract_num                 = 0,
 time_step_fract_den                 = 1,
 max_dom                             = 1,
 s_we                                = 1,      1,      1,
```

```
 e_we                                = 207,      424,      802,
 s_sn                                = 1,        1,        1,
 e_sn                                = 176,      379,      799,
 s_vert                              = 1,        1,        1,
 e_vert                              = 28,       28,       28,
 num_metgrid_levels                  = 38,
 num_metgrid_soil_levels             = 4,
 dx                                  = 30000,    10000,    3333.333,
 dy                                  = 30000,    10000,    3333.333,
 grid_id                             = 1,        2,        3,
 parent_id                           = 1,        1,        2,
 i_parent_start                      = 1,        34,       80,
 j_parent_start                      = 1,        35,       79,
 parent_grid_ratio                   = 1,        3,        3,
 parent_time_step_ratio              = 1,        3,        3,
 feedback                            = 1,
 smooth_option                       = 0,

&physics
 mp_physics                          = 2,        6,        6,
 ra_lw_physics                       = 1,        1,        1,
 ra_sw_physics                       = 1,        1,        1,
 radt                                = 30,       40,       40,
 sf_sfclay_physics                   = 1,        1,        1,
 sf_surface_physics                  = 1,        1,        1,
 bl_pbl_physics                      = 1,        1,        1,
 bldt                                = 0,        0,        0,
 cu_physics                          = 1,        1,        0,
 cudt                                = 5,        5,        5,
 isfflx                              = 1,
 ifsnow                              = 0,
 icloud                              = 1,
 surface_input_source                = 1,
 num_soil_layers                     = 5,
 maxiens                             = 1,
 maxens                              = 3,
 maxens2                             = 3,
 maxens3                             = 16,
 ensdim                              = 144,
 sst_update                          = 1,

&dynamics
 dyn_opt                             = 2,
 rk_ord                              = 3,
 w_damping                           = 0,
 diff_opt                            = 0,
```

```
 km_opt                  = 1,
 damp_opt                = 0,
 base_temp               = 290.,
 zdamp                   = 5000.,    5000.,    5000.,
 dampcoef                = 0.01,     0.01,     0.01,
 khdif                   = 0,        0,        0,
 kvdif                   = 0,        0,        0,
 smdiv                   = 0.1,      0.1,      0.1,
 emdiv                   = 0.01,     0.01,     0.01,
 epssm                   = 0.1,      0.1,      0.1,
 non_hydrostatic         = .true.,   .true.,   .true.,
 moist_adv_opt           = 1,        1,        1,
 scalar_adv_opt          = 1,        1,        1,
 use_baseparam_fr_nml    = .true.
 &bdy_control
 spec_bdy_width          = 9,
 spec_zone               = 1,
 relax_zone              = 8,
 specified               = .true.,   .false.,  .false.,
 spec_exp                = 0.33
 periodic_x              = .false.,  .false.,  .false.,
 symmetric_xs            = .false.,  .false.,  .false.,
 symmetric_xe            = .false.,  .false.,  .false.,
 open_xs                 = .false.,  .false.,  .false.,
 open_xe                 = .false.,  .false.,  .false.,
 periodic_y              = .false.,  .false.,  .false.,
 symmetric_ys            = .false.,  .false.,  .false.,
 symmetric_ye            = .false.,  .false.,  .false.,
 open_ys                 = .false.,  .false.,  .false.,
 open_ye                 = .false.,  .false.,  .false.,
 nested                  = .false.,  .true.,   .true.,

&namelist_quilt
 nio_tasks_per_group     = 0,
 nio_groups              = 1,
```